Cell Biomaterials

Article

TIMED: Temporal intervention with microparticle encapsulation and delivery—A programmed release system for post-myocardial infarction therapy

Graphical abstract

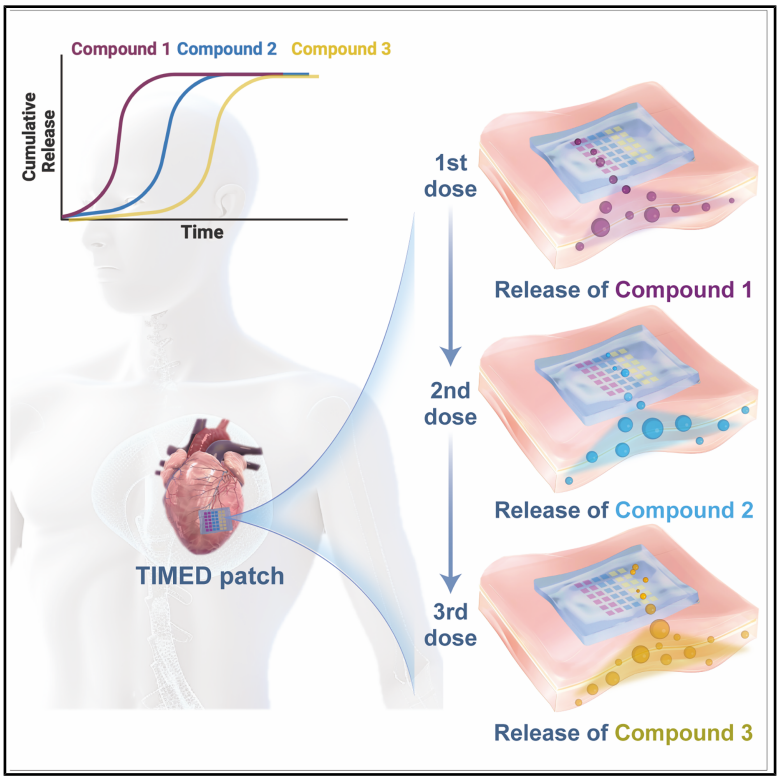

Highlights

- Programmable multi-phasic release via microparticles in a hydrogel patch
- Strong mechanics, biocompatibility, and storage stability for clinical use
- TIMED improves survival, restores function, and reduces injury *in vitro* and *in vivo*
- Modular, localized sequential therapy adaptable to broad clinical contexts

Authors

Erika Yan Wang, Elizabeth A. Calle, Binbin Ying, ..., Yi Liu, Robert Langer, Ana Jaklenec

Correspondence

rlanger@mit.edu (R.L.), jaklenec@mit.edu (A.J.)

In brief

This research addresses a significant unmet need in post-operative cardiac care by introducing TIMED, an implantable hydrogel patch with spatially patterned microparticles for programmable, sequential drug release. Validated in human stem cell-derived tissues and a rodent model, TIMED improved survival, reduced injury, and restored cardiac function. While demonstrated in a cardiac context, this versatile, translationally relevant biomaterial platform is broadly adaptable, highlighting innovation at the interface of materials science, bioengineering, and medicine.

Wang et al., 2026, Cell Biomaterials *2*, 100249
January 20, 2026
https://doi.org/10.1016/j.celbio.2025.100249

CellPress

Cell Biomaterials

CellPress

Article

TIMED: Temporal intervention with microparticle encapsulation and delivery—A programmed release system for post-myocardial infarction therapy

Erika Yan Wang,[1] Elizabeth A. Calle,[1,2] Binbin Ying,[1,3,4,10] Behnaz Eshaghi,[1] Linzixuan Zhang,[5] Xin Yang,[1] Stacey Qiaohui Lin,[1] Jooli Han,[1,6] Alanna G. Backx,[7] Yuting Huang,[1] Sevinj Mursalova,[1] Chuhan Joyce Qi,[1] Yi Liu,[8,9] Robert Langer,[1,5,*] and Ana Jaklenec[1,11,*]

[1]Koch Institute for Integrative Cancer Research, Massachusetts Institute of Technology, 77 Massachusetts Avenue, Cambridge, MA 02139, USA

[2]Department of Surgery, Massachusetts General Hospital, Boston, MA 02114, USA

[3]Department of Mechanical Engineering, Massachusetts Institute of Technology, 77 Massachusetts Avenue, Cambridge, MA 02139, USA

[4]Division of Gastroenterology, Hepatology and Endoscopy, Brigham and Women's Hospital, Harvard Medical School, Boston, MA 02115, USA

[5]Department of Chemical Engineering, Massachusetts Institute of Technology, 77 Massachusetts Avenue, Cambridge, MA 02139, USA

[6]Department of Biomedical Engineering, Seoul National University College of Medicine, Seoul 03080, South Korea

[7]The Division of Comparative Medicine, Massachusetts Institute of Technology, 77 Massachusetts Avenue, Cambridge, MA 02139, USA

[8]Ottawa Hospital Research Institute, Regenerative Medicine Program, Ottawa, ON K1H 8L6, Canada

[9]Department of Cellular and Molecular Medicine, Faculty of Medicine, University of Ottawa, Ottawa, ON K1H 8M5, Canada

[10]Department of Biomedical Engineering, University of Texas Southwestern Medical Center, Dallas, TX 75390, USA

[11]Lead contact

*Correspondence: rlanger@mit.edu (R.L.), jaklenec@mit.edu (A.J.)

https://doi.org/10.1016/j.celbio.2025.100249

THE BIGGER PICTURE Myocardial infarction (MI) remains one of the most pressing global health problems, leaving millions of patients with long-term cardiac dysfunction despite advances in acute surgical care. A major challenge is that the biological response to MI unfolds in distinct phases, yet most current therapies deliver drugs in a single burst, poorly aligned with these dynamic needs. This work introduces TIMED (temporal intervention with microparticle encapsulation and delivery), an implantable polymeric system. By combining spatially patterned microparticles within a hydrogel patch, TIMED achieves a programmable multi-phasic release profile. The system demonstrated strong mechanical performance and biocompatibility for surgical handling and long-term implantation and maintained stability during storage, showing potential for off-the-shelf clinical use.

First validated in human stem cell-derived cardiac tissues, our sequential treatment regimen delivered by TIMED enhanced survival and vascularization, while limiting fibrosis and supporting the biological logic of timed dosing. In a rodent MI model, TIMED treatment improved survival, reduced cardiac injury markers and infarct size, and restored heart function beyond what was achieved with equivalent dosing delivered by conventional intravenous therapy. These findings establish the first cardiac implantable polymeric platform with a programmable release profile, enabling advanced multi-dosing localized therapy. Beyond the demonstrated treatment regimen, the TIMED platform's precise control over drug combinations and release timing provides a framework for sequential treatment across broad therapeutic contexts.

SUMMARY

Myocardial infarction (MI) is a major global health challenge. Surgical interventions address the acute phase but often fail to support long-term recovery. Sequential post-operative drug delivery offers promise but is constrained by release methods. Here, we developed TIMED (temporal intervention with microparticle encapsulation and delivery), a polymeric device enabling programmed sequential release through spatially patterned microparticles in a tough hydrogel matrix. TIMED demonstrated excellent mechanical performance and biocompatibility for long-term implantation and retained strong stability after storage. A sequential dosing regimen aligned with the innate post-MI response was first validated in hiPSC-derived cardiac tissues, where it enhanced cell viability and vascularization while reducing collagen deposition. *In vivo*, delivery via the TIMED

Please cite this article in press as: Wang et al., TIMED: Temporal intervention with microparticle encapsulation and delivery—A programmed release system for post-myocardial infarction therapy, Cell Biomaterials (2025), https://doi.org/10.1016/j.celbio.2025.100249

improved survival, reduced injury markers and infarct size, and enhanced cardiac output, outperforming equivalent i.v. dosing. This work establishes a first-of-its-kind cardiac implantable polymeric platform with modular sequential release and provides a framework for programmed multi-dosing across diverse applications.

INTRODUCTION

Cardiovascular disease (CVD) is the leading cause of mortality on a global scale, with ischemic heart disease (IHD) being a primary subset.[1] One critical manifestation of IHD is myocardial infarction (MI),[2] which impacts around 3 million people globally each year and contributes to over 1 million annual deaths in the United States alone.[3] This condition arises from the cessation or reduction of blood flow to myocardial tissue, leading to cell death,[4] disrupted microvascular structure,[5] and fibrosis,[6] eventually compromising cardiac function.

Despite advancements in reperfusion strategies, such as percutaneous coronary intervention (PCI)[7,8] and coronary artery bypass grafting (CABG),[9,10] which aim to restore blood flow, these procedures often cannot fully reverse myocardial damage, resulting in suboptimal recovery.[8,9] Additionally, reperfusion itself can cause ischemia-reperfusion (IR) injury, necessitating further pharmacological intervention to mitigate its detrimental effects.[3] Post-procedural care frequently involves repeated medication administration and prolonged hospital stays, contributing significantly to healthcare costs and frequent hospital readmissions.[11] Subsequently, post-discharge 1-year rehospitalization rates exceeded 40% following PCI, with half of these occurring within the first 2 months, significantly contributing to overall healthcare expenditures.[11]

To optimize recovery post MI, there's a growing focus on direct cardiac delivery of therapeutic agents.[12–15] Various studies have demonstrated that localized delivery can significantly improve cardiac function compared with traditional systemic methods such as intravenous (i.v.) or oral administration.[12,15] Experimental studies and clinical trials have favored endovascular infusion, which involves catheter insertion via the femoral artery and guided delivery under fluoroscopy, as well as transendocardial injection, which employs a catheter with an injection needle for direct delivery into the heart muscle. However, these methods generally provide a single treatment opportunity and carry potential risks from repeated interventions, including catheter-related injuries. Alternatively, several preclinical studies have demonstrated that drug-loaded implantable devices, including cardiac patches, can continuously and locally deliver compounds such as vascular endothelial growth factor (VEGF) for angiogenesis,[16] interleukin-10 (IL-10) for anti-inflammation,[17] and transforming growth factor-beta (TGF-β) inhibitors for fibrosis inhibition.[18] However, most patches are limited to either single-drug delivery or a single-dose release, where all drugs are released simultaneously. Precise release profiles are often a challenge for hydrogels, making it difficult to control drug kinetics and prevent burst release, which can lead to rapid drug depletion, suboptimal therapeutic duration, increased systemic toxicity, and unintended off-target effects.[19–21] Achieving multidose pulsatile release is particularly challenging due to the need for sophisticated mechanisms to control different release kinetics through a single device over an extended period.

To address this pivotal challenge, we developed a platform called temporal intervention with microparticle encapsulation and delivery (TIMED). This hybrid polymeric system combines various drug-loaded microparticles within a tough hydrogel, with excellent mechanical performance and controlled release at dynamic surgical sites such as the heart. It introduces a first-of-its-kind approach to post-operative pharmacotherapy by delivering multiple therapeutics with precise temporal control, and aligning drug actions with the defined phases of regeneration and repair, thereby enhancing treatment efficacy.

Through extensive microparticle screening, we established a library of microparticles with precisely tuned release kinetics, spanning from 1 day to 1 month. This modular design allows for the customization of both drug combinations and release schedules, making it adaptable for a wide range of sequential therapeutic strategies. To validate this concept, we engineered the TIMED system to demonstrate a proof-of-concept sequential treatment based on the known temporal requirements of cardiac regeneration. Myocardial repair after infarction proceeds through tightly regulated phases: an early phase focused on preserving cardiomyocytes, a proliferative phase requiring angiogenesis to restore perfusion, and a remodeling phase where persistent TGF-β signaling promotes fibrosis.[22,23] Because processes that are beneficial in one phase can become detrimental in another, therapeutic success depends on synchronizing drug delivery with these temporal dynamics.[24] The system was engineered to release its encapsulated agents, neurogulin-1 (NRG1) for cell survival, VEGF for angiogenesis, and small molecule GW788388 for anti-fibrotic effects, at post-operative intervals of 1, 7, and 14 days, highlighting its ability to orchestrate a phased therapeutic intervention.

Following extensive *in vitro* and *in vivo* validation, our findings show that the TIMED system significantly increased cell survival and vascularization in human induced pluripotent stem cell (hiPSC)-derived cardiac spheres compared with hypoxic controls. In a rodent model of MI, it resulted in a significant increase in cardiac output, and a reduction in infarct size. Additionally, this system was stable for one month at 4°C, potentially easing clinical translation and enabling the development of an "off-the-shelf" product. Designed with a streamlined microfabrication process, this system aims to facilitate repeated administration on a single polymeric patch, potentially improving long-term recovery and alleviating the high costs associated with follow-up procedures.

RESULTS

Design and fabrication of the TIMED patch

The TIMED patch is designed as a polymeric device for safe application at the surgical site. It features high modularity through patterning and encapsulation of an array of microcarriers with different pulsatile kinetics at controlled intervals. This supports repeated administration of single or multiple drugs,

Please cite this article in press as: Wang et al., TIMED: Temporal intervention with microparticle encapsulation and delivery—A programmed release system for post-myocardial infarction therapy, Cell Biomaterials (2025), https://doi.org/10.1016/j.celbio.2025.100249

CellPress

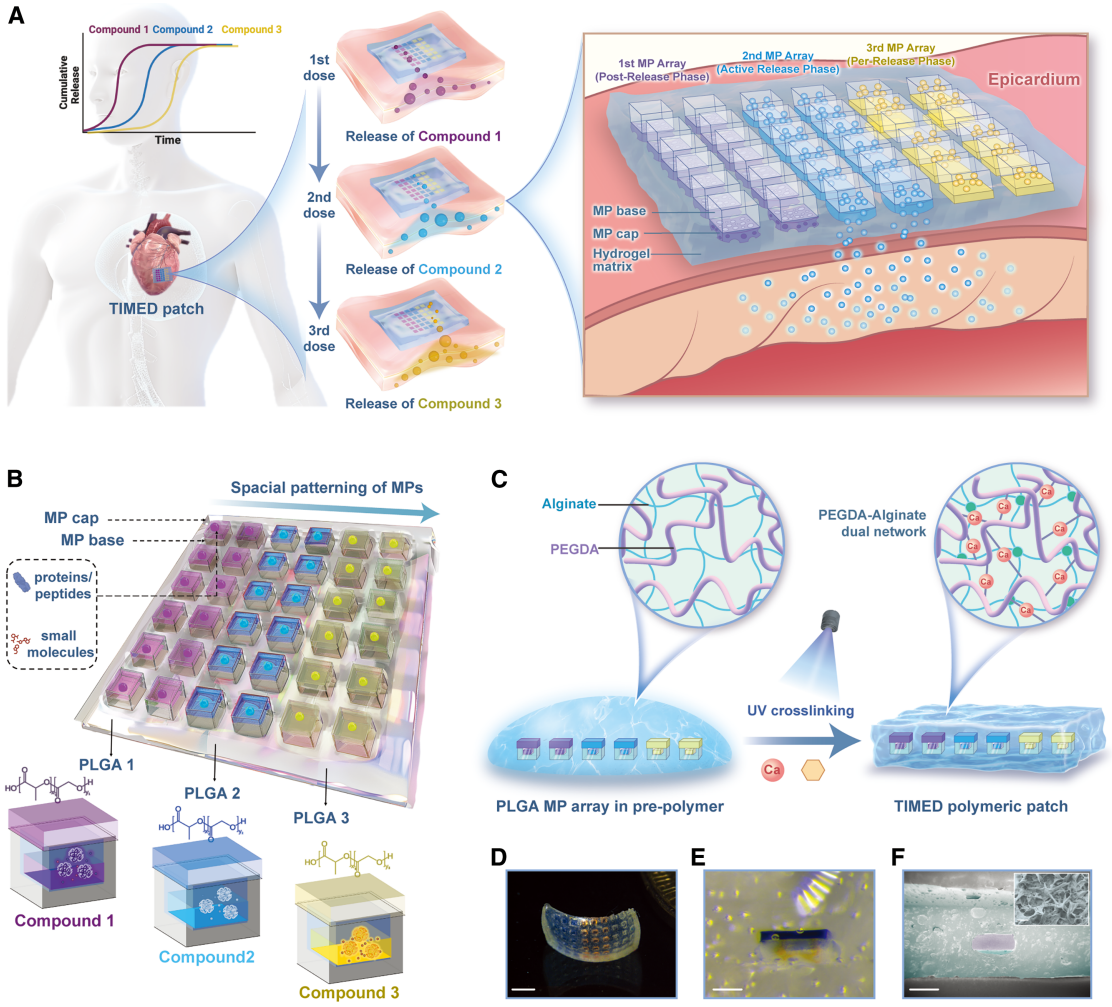

Figure 1. Design and fabrication of the TIMED system

(A) Schematic illustrating the multi-phasic therapeutic delivery profile of the TIMED system implanted on the heart, with sequential release of different compounds shown in different colors. The enlarged view illustrates the phase-specific release, where therapeutic agents are released through the particle cap into the heart muscle.

(B) 3D configuration of the drug-loaded PLGA MP array, highlighting various compounds encapsulated in spatially patterned MPs composed of different PLGA variants.

(C) Polymerization of the dual-network hydrogel patch for MP encapsulation and TIMED patch assembly.

(D) Optical image of a TIMED patch loaded with microparticles. Scale bar, 2 mm.

(E) Optical image of a dextran fluorescein isothiocyanate (FITC) dye-loaded microparticle, encapsulated within the TIMED patch. Scale bar, 200 μm.

(F) Scanning electron microscopy (SEM) image of the hydrogel matrix and a tightly encapsulated MP for detailed structural observation. The microparticle is pseudo-colored in purple for differentiation from the hydrogel. Scale bar, 400 μm. The hydrogel network is shown in the inset at a higher magnification. Scale bar, 100 μm.

with customizable schedules for precise temporal control (Figure 1A).

We selected polylactic-co-glycolic acid (PLGA), a polymer recognized for its biocompatibility,[25,26] as the substrate for microparticle fabrication. PLGA films were molded into base configurations with a central reservoir for drug loading, and then thermally bonded with PLGA caps to form hermetically sealed particles (Figures 1B and S1). Contrasting with our previous single microparticles (MPs) administration approach,[27,28] we adopted a spatial patterning technique to create a bulk system comprising a diverse array of MPs. This allows precise deposition of different PLGA materials with distinct release profiles within a single device.

To secure placement of PLGA microparticles at the tissue site, a tough hydrogel network was engineered to provide a robust matrix that effectively immobilized the MPs, preventing their migration and enabling localized delivery over an extended timeframe. Achieving sufficient toughness and elasticity is imperative for embedding the particles securely within the hydrogel matrix, thereby preventing dislocation and ensuring long-term immobilization on the dynamic cardiovascular tissue. A double-network hydrogel composed of alginate and a high molecular weight

Please cite this article in press as: Wang et al., TIMED: Temporal intervention with microparticle encapsulation and delivery—A programmed release system for post-myocardial infarction therapy, Cell Biomaterials (2025), https://doi.org/10.1016/j.celbio.2025.100249

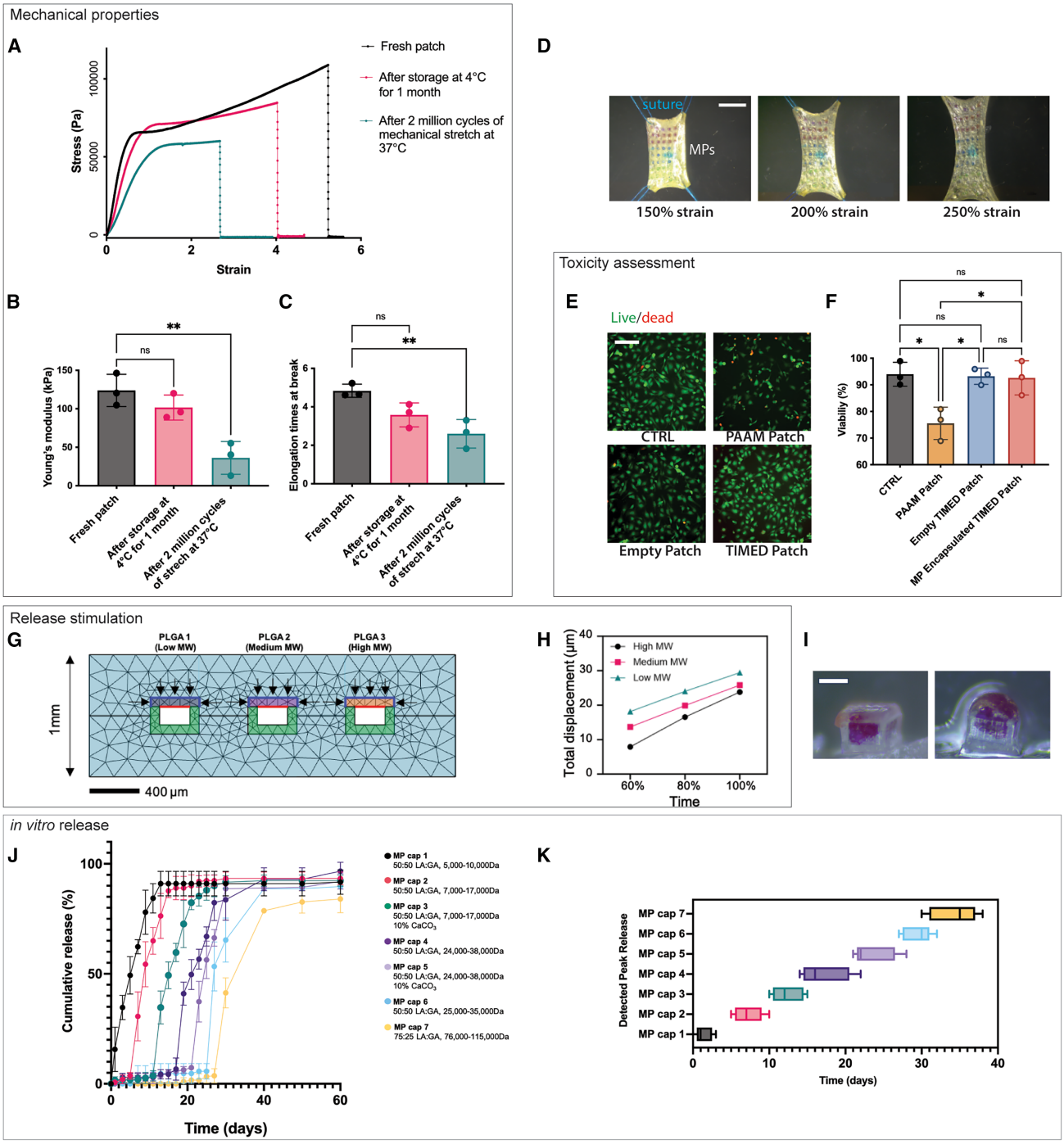

Figure 2. Mechanical, biocompatibility, and release characterization of the TIMED patch

(A) Representative stress-strain curves from tensile testing of TIMED patches in a swollen state: freshly prepared, stored for 1 month at 4°C, and after 2 million stretch cycles at 37°C.

(B) Analysis of Young's modulus derived from tensile testing assessments (n = 3).

(C) Measurement of elongation at the break point from tensile testing assessments. *n* = 3.

(D) Images display the TIMED patch affixed with four 6-0 Prolene suture stitches at each corner, demonstrating its resistance to various strains without tearing. Scale bar, 6 mm.

(E) Representative fluorescent images of HUVECs after 4-day culture with and without patch placement for toxicity assessment. Calcein acetoxymethyl ester (AM) and ethidium homodimer-1 were used to label live and dead cells, respectively. Scale bar, 200 μm.

(F) Quantitative analysis of cell viability from (E). *n* = 3.

(legend continued on next page)

(MW) poly(ethylene glycol) diacrylate (PEGDA) formulation was optimized for its exceptional mechanical strength, stretchability, biocompatibility, and rapid UV crosslinking (Figure 1C). To envelop the PLGA MPs within the hydrogel matrix, we employed a bilayer composite encapsulation technique. This strategy effectively prevented particle detachment during implantation and long-term placement, avoiding adverse foreign reactions and payload loss (Figures S2A and S2B). Following this procedure, an engineered elastomeric patch was formed (Figure 1D), with microparticles securely embedded within the matrix (Figures 1E and 1F).

Mechanical properties and biocompatibility of the TIMED patch for long-term implantation

The mechanical properties of an implantable system are crucial for its performance on dynamic cardiac tissue. Our tests revealed an initial Young's modulus of approximately 120 kPa and excellent stretchability exhibiting 480% elongation (Figures 2A–2C and S2C), falling within the suitable range for placement on various biological surfaces, including a contracting heart, a notably challenging site for implantation owing to its dynamic nature.[29] This modulus ensures that the patch remains sufficiently flexible to adapt to the heart's movements while maintaining its structural integrity.[30–32] The mechanical toughness also enables the hydrogel to withstand the tension applied by surgical sutures, including Prolene (polypropylene) and silk, without tearing (Figure 2D). Alternatively, a hydrogel adhesive leveraging a combination of physical and chemical bonds can be utilized for tissue bonding where sutures are difficult to apply[33] (Figures S2H–S2J). Because the alginate/PEGDA hydrogel is soft and viscoelastic relative to the active myocardium, it conforms to the epicardial surface without constraining motion, and its mechanical effect is not expected to differ depending on the stage of the cardiac cycle. After 1 month of storage at 4°C, the Young's modulus was maintained at around 85% of its initial strength, remaining above 100 kPa and 230% elongation at break (Figures 2A–2C and S2D). Despite this decline in modulus relative to fresh patches, these values remain well within a range that supports surgical handling and cardiac performance,[29,34] showing potential for off-the-shelf feasibility for clinical use.

To simulate long-term cardiac application, we employed a testing method using a balloon system actuated by a ventilator (Figure S2E). This setup mimicked cardiac contractions by subjecting the hydrogel patch to 2 million cycles of stretching at 200% strain, exceeding the typical strain experienced by the heart's movements over approximately 1 month. These tests were conducted in humidified conditions at 37°C to replicate the environment of the chest cavity. Although a significant decline in modulus and elongation was observed after cyclic loading, as expected for PEG-based systems under prolonged fatigue,[36–38] the patch maintained structural integrity throughout testing, with Young's modulus remaining above 35 kPa and elongation at break exceeding 200% post fatigue, values within the physiologic range required to accommodate cardiac contraction (Figures 2A–2C). Consistently, patches stored for 1 month at 4°C withstood >2 million fatigue cycles and retained mechanical properties comparable to fresh patches tested under the same conditions (Figures S2F and S2G).

To assess the thermal properties of this system, we conducted differential scanning calorimetry (DSC) (Figure S3). The glass transition temperatures (Tg) of the PLGA microparticles and hydrogel remained constant at approximately 51.5°C ± 1°C and 60.8°C ± 1°C, respectively, well above physiological body temperature, ensuring no thermal-induced morphological deformations, thereby preventing unintended release of encapsulated agents.[39] The consistent Tg values through various processing steps, and the presence of two distinct peaks in the DSC results, demonstrate compatibility between the MP and hydrogel components (Figure S3A). This indicates that the engineering process preserves the individual physical characteristics of each component, ensuring they can function independently within the dual-carrier system without compromising their specific drug delivery functions.[40]

To evaluate the system's biocompatibility and toxicity profile, we utilized human umbilical vein endothelial cells (HUVECs) within a transwell system. This model served as an initial proxy for assessing the interaction between the engineered patch and the endothelial lining of blood vessels, which is essential for various organ systems.[41] The results indicated a markedly low cytotoxicity for the TIMED patch, demonstrating its biocompatibility when compared with polyacrylamide (PAAM) patches, a commonly referenced tough hydrogel material.[42,43] These results validated the patch's enhanced safety profile for potential implantation (Figures 2E and 2F). To further evaluate its implantability, we examined the TIMED patch's swelling behavior under various physiological conditions. The patch reached its equilibrium swelling ratio of 40% within hours, allowing for stable handling during implantation and sufficient time to conform to surrounding tissues (Figure S4A). Upon swelling, Young's modulus exhibited a statistically significant 10%–15% reduction relative to the dry state; however, the magnitude of this change is

(G) Computational simulation of drug-release kinetics from three sets of PLGA microparticles capped with polymers of differing molecular weights. Distinct colors represent the different PLGA cap formulations. The model couples a solid mechanics module with a poroelasticity module, with deformation governed by coupled equations.[35]

(H) Temporal simulation of particle deformation correlating with variations in PLGA molecular weight, illustrating the role of polymer molecular weight in modulating particle deformation.

(I) Optical image of a microparticle loaded with Alexa 694 dextran dye before and after cap deformation, capturing drug release initiated by cap deformation. Scale bar, 300 μm.

(J) Release kinetics of dextran dyes from MPs fabricated with a panel of different cap materials, varying molecular weight and lactide-to-glycolide ratio. $n = 3$.

(K) Initial time of peak release detected from each MP composition. $n = 3$.

Data represent the mean ± SD. Ordinary one-way ANOVA (Sidak's multiple comparisons test) were used. p values are represented by: $^{*}p \leq 0.05$; $^{**}p \leq 0.01$; $^{***}p \leq 0.001$; $^{****}p \leq 0.0001$; ns, not significant.

Please cite this article in press as: Wang et al., TIMED: Temporal intervention with microparticle encapsulation and delivery—A programmed release system for post-myocardial infarction therapy, Cell Biomaterials (2025), https://doi.org/10.1016/j.celbio.2025.100249

modest compared with the several-fold declines often reported in softer hydrogel systems, which can markedly reduce mechanical integrity.[37,38,44] Elasticity remained largely preserved with no significant reduction (Figures S2F and S2G). Degradation tests showed that the PLGA microparticles dissolved within ~3 months, ensuring retention during the therapeutic window (Figures S4B–S4D). In contrast, the PEGDA/alginate matrix displayed a slow degradation profile, remaining intact at 6 months and markedly thinned by 12 months (Figures S4B and S4C). Although gradual degradation is expected to continue beyond 1 year, the matrix is designed for biocompatibility and is not anticipated to impair cardiac function.

Simulation and screening of temporally controlled drug-release profiles

To elucidate the release kinetics for a tunable multimodal release system, we integrated computational modeling and *in vitro* assays on the TIMED patch. Utilizing COMSOL Multiphysics (Figure 2G), we identified the effect of microparticle cap deformation on drug-release kinetics (Figure 2H), positioning MP cap deformation as an adjustable parameter to modulate release rates in a consistent hydrogel matrix. This finding aligned with our observation that release initiation correlates with cap deformation (Figure 2I). The analysis revealed that the mechanical properties of the PLGA in the cap, influenced by its MW, significantly dictate its deformation, which in turn triggers drug release, making MW a key adjustable factor for customizing release patterns from microparticles embedded in the hydrogel matrix (Figures 2H and S5).

To validate the release modularity, *in vitro* screenings were conducted using a transwell model, where the MPs released the payloads into a release buffer beneath the insert, simulating the physiological fluid environment (Figure S6A). The TIMED patch contained PLGA MPs, loaded with fluorescent molecules conjugated to 10 kDa dextran as a model compound. Fluorescent intensity in the release buffer was quantified to assess the release kinetics from each PLGA variant. We assessed a panel of MP cap formulations, varying parameters such as MW and lactide-to-glycolide ratio (Figure 2J). We observed clearly distinct release profiles with pulsatile kinetics (Figure 2J), with peak release times ranging from 1 day to 1 month (Figure 2K), achieved by patterning MPs with different cap materials in the same patch. The segregated release profiles from different cap materials, exhibited consistency across two selected MP base materials, indicating the cap material as a customizable component for attaining engineering consistency in drug-release behavior (Figure S6). By leveraging a well-characterized MP library with defined release kinetics, the system enables a highly adaptable framework for programmable sequential treatment strategies.

For functional stability after implantation, we further evaluated whether cyclic myocardial deformation affects drug-release kinetics. The TIMED patch was subjected to dynamic mechanical stretching at 300 beats per minute (bpm), mimicking the rat heart rate, at 37°C, with a 53.5% strain, which is well above typical cardiac deformation.[34] Drug-release profiles measured under both static and dynamic conditions showed no significant differences (Figure S7). These results confirm that controlled drug release is primarily dependent on the cap material's MW rather than external mechanical strain, ensuring consistent and predictable drug delivery despite the contractile forces of the cardiac environment. Additionally, the hydrogel matrix serves as a diffusion medium, enabling uniform drug distribution across the patch. Imaging of fluorescently labeled dextran confirmed that diffusion from a single particle array extends throughout the patch, ensuring even exposure to the underlying tissue (Figure S8).

A sequential drug delivery strategy for cardiac regeneration using the TIMED system

To develop a protocol for post-MI combination therapy, we designed a treatment regimen involving the precise delivery of multiple molecules at designated time points. Each molecule was selected from preclinical studies highlighting their temporal effects in cardiac repair.[45–47] NRG1, known for its cardioprotective effects, is often administered acutely post MI to minimize immediate cardiac apoptosis.[48] VEGF is delivered 1 week post MI during the peak of the angiogenic phase, to support vessel formation and tissue repair.[23] Last, GW788388, a small molecule inhibitor to TGF-β is usually introduced around week 2 to mitigate fibrosis, aligning with the transition from beneficial to detrimental TGF-β signaling in post-MI wound healing[49] (Figure 3A). This regimen was used as a proof of concept to validate the potential of phased delivery systems to improve therapeutic outcomes by aligning drug delivery schedules with biological repair processes.

Each of the therapeutic compounds was encapsulated within distinct segments of PLGA MP arrays, all housed within the same patch. The TIMED patch facilitated the co-loading of excipients within MPs to preserve the stability and bioactivity of the protein compounds during storage and release (Figure 3B). After screening multiple excipients and their combinations, including bovine serum albumin (BSA), trehalose (Tre), and heparin (Hp) for each therapeutic agent, we selected formulations that demonstrated a recovery rate above 85%, indicating the preservation of the initial therapeutic activity post fabrication, for inclusion in the final system (Figure S9). These tailored excipient formulations enhanced the biostability of the system during fabrication and storage, maintaining over 85% bioactivity post particle sealing and hydrogel encapsulation, over 80% after 1-month storage at 4°C, and retaining more than 70% after 2 weeks of incubation in physiological conditions at 37°C (Figure 3C). Bioactivity was evaluated using functional assays, including NRG1-induced cell proliferation, VEGF receptor activation, and TGF-β inhibition, to confirm the preservation of each component's biological activity. After dispensing in the same patch and patterning with caps for targeted release time, each component underwent *in vitro* assessment using enzyme-linked immunosorbent assay (ELISA) (Figures 3D and 3E) or liquid chromatography-mass spectrometry (LC-MS) (Figure 3F). The results indicated that each component exhibited peak release at the designated time points, days 1–3, days 7–9, and days 12–14, aligning with its targeted therapeutic windows.

To assess the efficacy of this combination therapy, we established an *in vitro* model of micro-cardiac spheres. These spheres were constructed by co-culturing human induced pluripotent stem cell (hiPSC)-derived cardiomyocytes(CMs) with human

Please cite this article in press as: Wang et al., TIMED: Temporal intervention with microparticle encapsulation and delivery—A programmed release system for post-myocardial infarction therapy, Cell Biomaterials (2025), https://doi.org/10.1016/j.celbio.2025.100249

CellPress

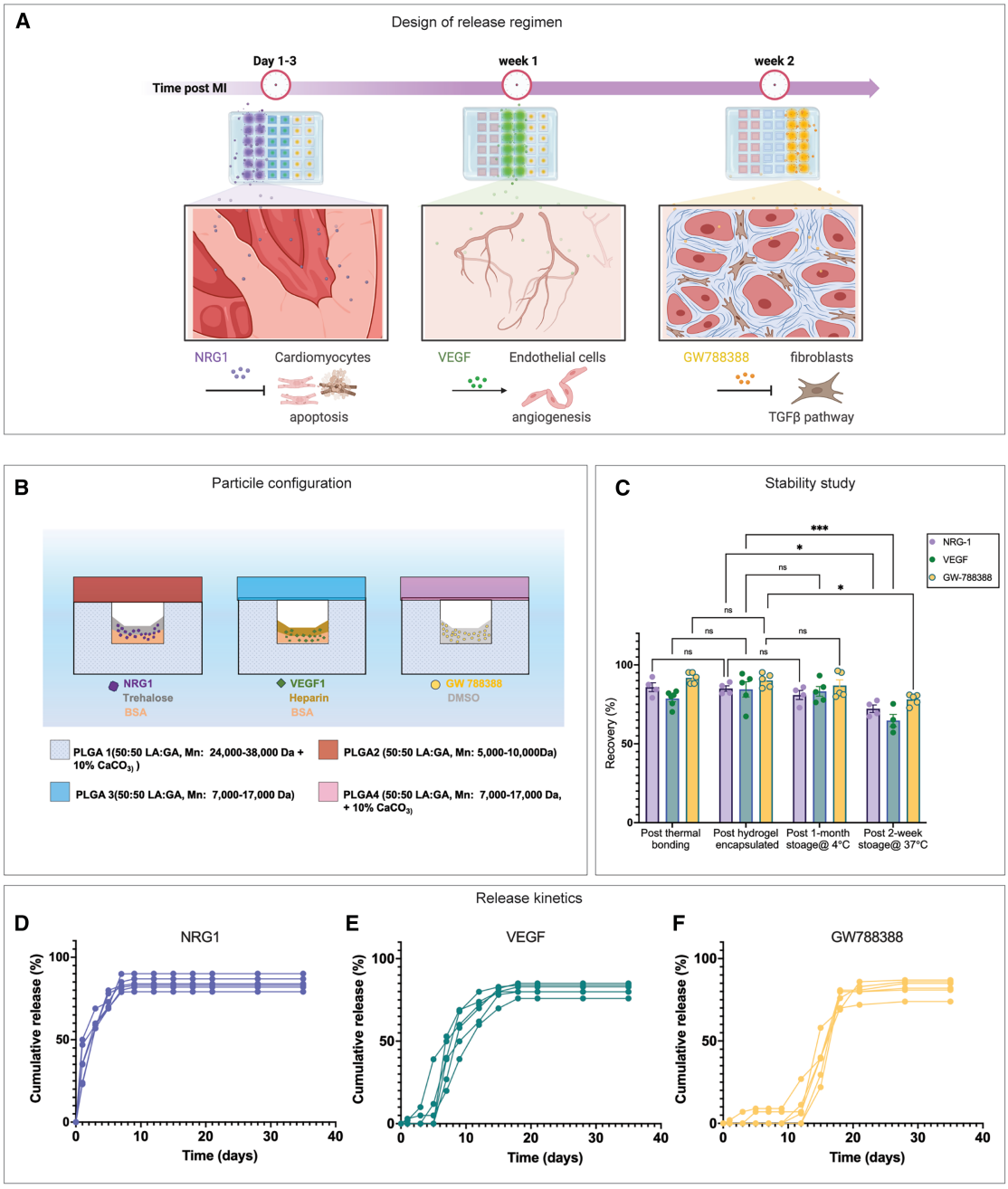

Figure 3. Design and release study of a proof-of-concept cardiac combination therapy with the TIMED system

(A) Design of the sequential therapy employing three drugs, each administered at specific time points post MI to target different repair pathways within their respective time windows.

(B) Configuration of discrete PLGA microparticles within the patch, where each particle consists of a base with a central reservoir for therapeutic loading and a matching cap sealed by thermal bonding. Distinct sets of microparticles were used to encapsulate NRG1, VEGF, or GW788388, together with optimized excipients, and assembled within the same patch array.

(C) Recovery rate of each compound, determined as the ratio of retained to initial bioactivity, following thermal bonding, hydrogel encapsulation, either 1-month storage at 4°C or 2-week incubation at 37°C of freshly prepared patches with the optimized excipient formulation. Bioactivity was assessed through compound-specific assays to confirm activity retention. $n \geq 6$.

Data represent the mean ± SD, ordinary two-way ANOVA (Sidak's multiple comparisons test) were used. p values are represented by $^{*}p \leq 0.05$; $^{**}p \leq 0.01$; $^{***}p \leq 0.001$; $^{****}p \leq 0.0001$; ns, not significant.

(D–F), Release kinetics of each therapeutic agent from the TIMED patch, using ELISA (NRG1 and VEGF) and LC-MS (GW788388) for quantitative analysis. $n \geq 5$.

Please cite this article in press as: Wang et al., TIMED: Temporal intervention with microparticle encapsulation and delivery—A programmed release system for post-myocardial infarction therapy, Cell Biomaterials (2025), https://doi.org/10.1016/j.celbio.2025.100249

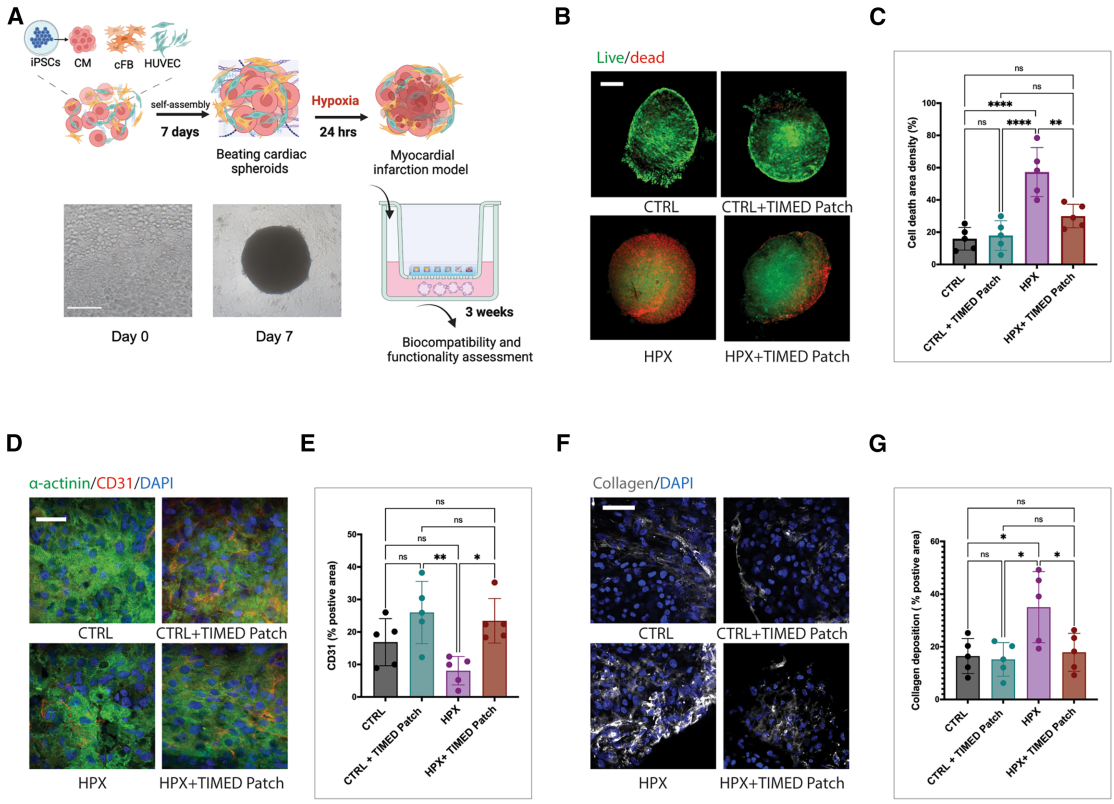

Figure 4. *In vitro* validation of a proof-of-concept cardiac combination therapy with TIMED system

(A) Schematics of the experimental setup of *in vitro* efficacy assessment using a cardiac sphere model, along with bright-field images of cardiac spheres after seeding (day 0) and self-assembly (day 7).

(B) Representative images showing live-dead staining of cardiac spheres from different groups. Scale bar, 250 μm.

(C) Quantitative analysis of cell death per mm^2 tissue area. $n = 5$.

(D) Representative images of cardiac spheres stained with α-actinin and CD31 to evaluate cellular composition and angiogenesis. Scale bar, 10 μm.

(E) Quantification of CD31 coverage, indicative of the extent of neovascularization within the cardiac spheres. $n = 5$.

(F) Representative images of cardiac spheres stained for collagen to assess fibrotic deposition. Scale bar = 10 μm.

(G) Quantitative analysis of collagen coverage as a metric for fibrosis within each tissue sample. $n = 5$.

Data represent the mean ± SD. Ordinary one-way ANOVA (Sidak's multiple comparisons test) were used. p values are represented by: $^{*}p \leq 0.05$; $^{**}p \leq 0.01$; $^{***}p \leq 0.001$; $^{****}p \leq 0.0001$; ns, not significant.

ventricular cardiac fibroblasts (CFBs) and HUVECs, aiming to emulate the cardiac tissue composition *in vitro* (Figure 4A).[50] These cells were selected as they constitute the primary structural and functional cellular framework of the myocardium, making them a relevant model for cardiac function.[51,52] Furthermore, they enable targeted assessment of therapeutic responsiveness, cardiomyocytes allow evaluation of NRG1's cardioprotective effects, endothelial cells support the analysis of VEGF-induced angiogenesis, and fibroblasts provide a model for assessing the anti-fibrotic effects of TGF-β inhibition.[48,53]

To simulate acute MI-like conditions, the cardiac spheres were subjected to 24 h of hypoxia with 1% O_2. The drug-loaded TIMED patch was subsequently positioned on a transwell insert above the cardiac tissue cultures and maintained for a period of 4 weeks along with control groups. Treatment with the drug-loaded TIMED patch resulted in a 47% decrease in dead cells post hypoxia compared with untreated controls (Figures 4B and 4C). Additionally, this treatment group exhibited an approximately 2-fold increase in CD31-positive cells (Figures 4D and 4E), and a 51% reduction in collagen deposition compared with the hypoxic tissues (Figures 4F and 4G). These results serve to validate our rationale regarding the effectiveness of timed therapy in promoting cardiac repair.

To validate the enhanced efficacy of timed release over single-dose administration and optimize the sequential release regimen, we initially screened multiple treatment strategies, including single-phase release of NRG1, VEGF, and TGF-β inhibitors (pirfenidone and GW788388), combined single-dose administration of all agents, and staged release via the TIMED system. The optimized sequential regimen (NRG1, VEGF, and GW788388) demonstrated a consistent increase in cell viability across 3 weeks of cultivation (Figure S10A).

While previous studies have shown that hypoxia enhances the angiogenic capacity of hiPSC-derived endothelial cells in short-term *in vitro* assays,[54] we employed a long-term tri-cellular 3D cardiac sphere model comprising cardiomyocytes, endothelial

Please cite this article in press as: Wang et al., TIMED: Temporal intervention with microparticle encapsulation and delivery—A programmed release system for post-myocardial infarction therapy, Cell Biomaterials (2025), https://doi.org/10.1016/j.celbio.2025.100249

cells, and fibroblasts to better approximate the *in vivo* cardiac microenvironment. Our findings agree with reports that fibroblast-mediated extracellular matrix remodeling and shifts in paracrine signaling can diminish transient pro-angiogenic effects over prolonged culture.[55,56] Notably, TIMED therapy enhanced vascularization beyond VEGF-only treatment (Figure S10B). Furthermore, TIMED treatment led to collagen reduction, while maintaining a more stabilized collagen matrix network compared with GW788388-only treatment (Figure S10D).

To gain more insight, we performed quantitative reverse-transcription PCR (RT-qPCR) analysis on key genes regulating cell survival, stress response, fibrosis, and angiogenesis. Hypoxia-inducible factor 1-alpha (HIF-1α) upregulation under hypoxia confirmed the model's validity in replicating myocardial ischemia.[57] Compared with combined single-dose administration, the TIMED patch significantly reduced caspase-3, B-type natriuretic peptide (BNP), and interleukin-6 (IL-6), likely because staggered release prevented uncontrolled peak concentrations that exacerbate stress-induced responses.[58–60] It also provided superior fibrosis regulation, with a marked decrease in TGF-β, collagen type I alpha 1 chain (COL1A1), and matrix metalloproteinase 2 (MMP2) expression. Notably, TIMED therapy enhanced angiogenesis, with higher platelet and endothelial cell adhesion molecule 1 (PECAM1) expression than single-dose VEGF administration.[61] These results explain the observed phenotypes, demonstrating that sequential, timed delivery optimally activates repair pathways, while preventing stress-induced responses, which are often exacerbated in single-dose treatments due to uncontrolled peak drug concentrations (Figure S11).

Implantation of the TIMED patch in a rodent model of MI

To validate the therapeutic benefits of the TIMED system in a more complex biological system *in vivo*, we established a rodent model of MI via left anterior descending (LAD) artery ligation.[62] The TIMED patch was surgically implanted onto the epicardium following induction of MI to deliver targeted drug therapy directly to the infarct site (Figures 5A and S14).

To evaluate treatment efficacy, in addition to the group receiving TIMED patch implantation, we included a control group with LAD ligation only to replicate untreated MI, a sham group with LAD ligation and placement of an empty patch to offset procedural and material effects. An additional group was included, receiving the equivalent three medications (NRG1, VEGF, and GW 788388) via tail vein injections at days 1, 7, and 14, for comparison with conventional i.v. treatment in the designed regimen (Figure 5A). Each group was sex-matched for comprehensive assessment and clinical inclusivity.[63] A panel of assessments, including physiological evaluation, weight measurement, cytokine analysis from tail vein blood sampling, and echocardiography, was conducted both before and after the surgical procedure, at multiple time points until reaching the 4-week endpoint (Figure 5A).

The group with TIMED patch implantation showed the highest survival rates among all animals in the study (Figure 5B), leading to 33% increase compared with untreated MI and a 17% increase compared with i.v. injection at the 4-week endpoint. The enhancement in survival observed in the empty patch group compared with untreated MI may be, in part, attributed to a mechanical support conferred by the patch's substrate, which helps stabilize the weakened cardiac wall post MI.[64,65] The TIMED patch group maintained above 90% of their initial weight at the 4-week endpoint, demonstrating better post-operative weight retention compared with the MI group (Figure S12). This suggests that localized delivery of therapeutics to the infarct site may alleviate catabolic effects associated with stress responses post-myocardial injury. Consequently, it could potentially preserve body mass and enhance overall clinical outcomes.[66]

Cardiac injury markers including troponin I, troponin T, and creatine kinase-myocardial band (CK-MB),[67] were quantitatively measured using Luminex assay to monitor myocardial damage (Figure 5C). In our study, all groups experienced a rise in these markers during the initial 24 h post MI. However, the group treated with the TIMED patch showed an average reduction of over 50% in all three cardiac biomarkers, validating the release of NRG1, which is known for promoting cardiomyocyte survival.[46,68]

To validate *in vivo* release kinetics, serum samples were concentrated at multiple time points to enhance detectability, given the expected low systemic concentrations of the encapsulated compounds. All therapeutic agents were successfully detected within the anticipated release window, confirming that their pharmacokinetics align with the designed multi-phasic release profile (Figure 5D). To evaluate therapeutic delivery to the myocardium, the TIMED patch was loaded with dye-labeled 40 kDa dextran, selected to approximate the diffusion characteristics of protein-sized therapeutics. Fluorescence was detected from the epicardium to the endocardium, confirming penetration into deeper myocardial layers. Co-localization with cardiomyocytes confirmed targeted delivery, ensuring therapeutics reached the intended cells for cardiac repair (Figure5E). Additionally, *in vivo* imaging system (IVIS) imaging of major organs confirmed that drug distribution remained localized to the heart, with no detectable signal in secondary organs, including the lungs, liver, spleen, and kidneys, indicating minimal systemic exposure and a low risk of off-target effects (Figure S13).

Functional cardiac assessments were conducted weekly using echocardiography to monitor the health and functionality of the heart post intervention (Figure S15A). Notably, in the group with MI, the movement of the left ventricular wall became flattened, indicating reduced cardiac contractility. This can be visualized in the motion-mode (M-mode) of echocardiography (Figure S15B). However, the group with the TIMED patch exhibited a pronounce reduction in this alteration, noticeably observed in M-mode recording (Figure S15B). Key parameters including ejection fraction (EF) and fractional shortening (FS), were monitored to assess cardiac function over time. The group with TIMED patch implantation exhibited statistically significant long-term improvements, with more than a 15% increase in both EF and FS compared with the MI group and i.v. injection control group at endpoint (Figures 6A and 6B).

At 4 weeks, all hearts were procured for endpoint assessments. The patches remained intact and securely affixed to the myocardium upon reopening of the chest cavity (Figure S16). Additionally, our observations revealed a significant decrease in surgical adhesion for the TIMED patch compared with other

Please cite this article in press as: Wang et al., TIMED: Temporal intervention with microparticle encapsulation and delivery—A programmed release system for post-myocardial infarction therapy, Cell Biomaterials (2025), https://doi.org/10.1016/j.celbio.2025.100249

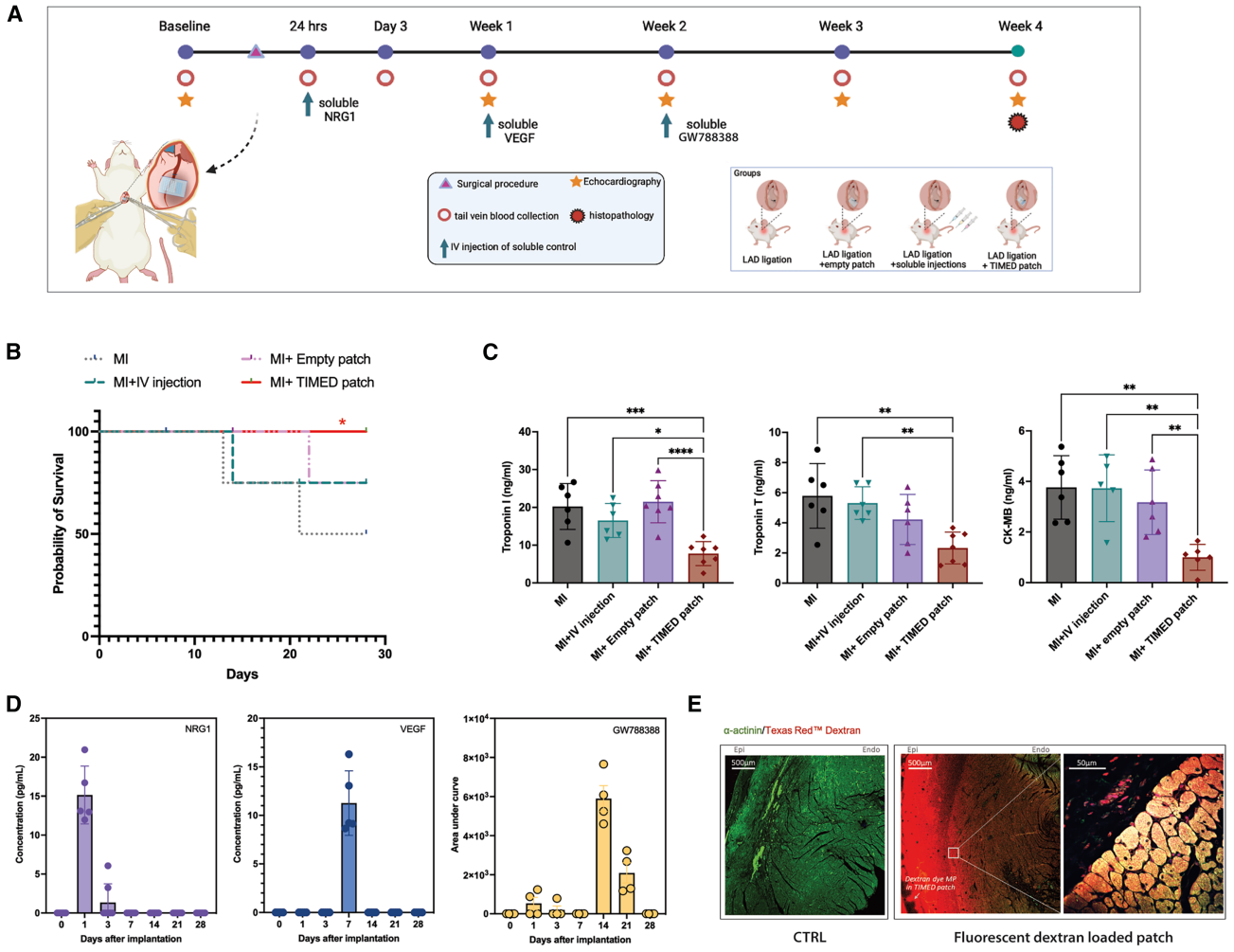

Figure 5. ***In vivo*** **validation of TIMED system release and therapeutic distribution following implantation in rats post MI**

(A) Experimental design including surgical procedures and pre- and post-surgical assessments.

(B) Kaplan-Meier curve depicting survival rates over the duration of the *in vivo* study across different groups. $n = 6$.

(C) Quantitative analysis of cardiac injury biomarkers 24-h post MI, including troponin I, troponin T, and creatine kinase-myocardial band (CK-MB), analyzed from serum samples. $n \geq 5$.

Data represent the mean ± SD. Ordinary one-way ANOVA (Sidak's multiple comparisons test) were used. p values are represented by: $^{*}p \leq 0.05$; $^{**}p \leq 0.01$; $^{***}p \leq 0.001$; $^{****}p \leq 0.0001$; ns, not significant.

(D) *In vivo* release kinetics of NRG1 and VEGF, quantified by ELISA after serum concentration, and GW788388 measured via LC-MS. $n \geq 4$.

(E) Cardiac tissue imaging showing myocardium from control and TIMED patch-implanted hearts. The patch was loaded with 40 kDa Texas Red-conjugated dextran to visualize molecular diffusion through cardiac tissue. Co-staining with α-actinin highlights cardiomyocytes, confirming targeted delivery and tissue penetration.

groups (Figure S17). The medicated patch maintained a smooth surface upon examination after the 4-week period, suggesting reduced fibrotic encapsulation. In contrast, patches without drugs developed fibrotic capsules covering the patch and adhesion to the chest (Figures S16 and S17). This drastic difference serves as evidence supporting the effectiveness of timed release of the TGF-β inhibitor in reducing collagen deposition.

Histopathological analysis corroborated the therapeutic efficacy of the patch. In the group treated with the TIMED patch, a 51% reduction in infarct size and a 66% enhancement in ventricular wall thickness as evidenced by Masson's trichrome staining (Figure 6C), and hematoxylin and eosin (H&E) staining (Figure S18A).

The efficacy of this approach was further validated through immunostaining for the cardiomyocyte marker alpha-actinin and the endothelial marker CD31 (Figure 6D). The analysis revealed a 53% increase and improved arrangement of cardiomyocytes within the infarct region, with the myocardium of the heart in the medicated patch group closely resembling the architecture of healthy myocardium, as opposed to the disorganized and sparse distribution observed in untreated infarct zones (Figures 6D, 6G, and S18B). Furthermore, a

Please cite this article in press as: Wang et al., TIMED: Temporal intervention with microparticle encapsulation and delivery—A programmed release system for post-myocardial infarction therapy, Cell Biomaterials (2025), https://doi.org/10.1016/j.celbio.2025.100249

CellPress

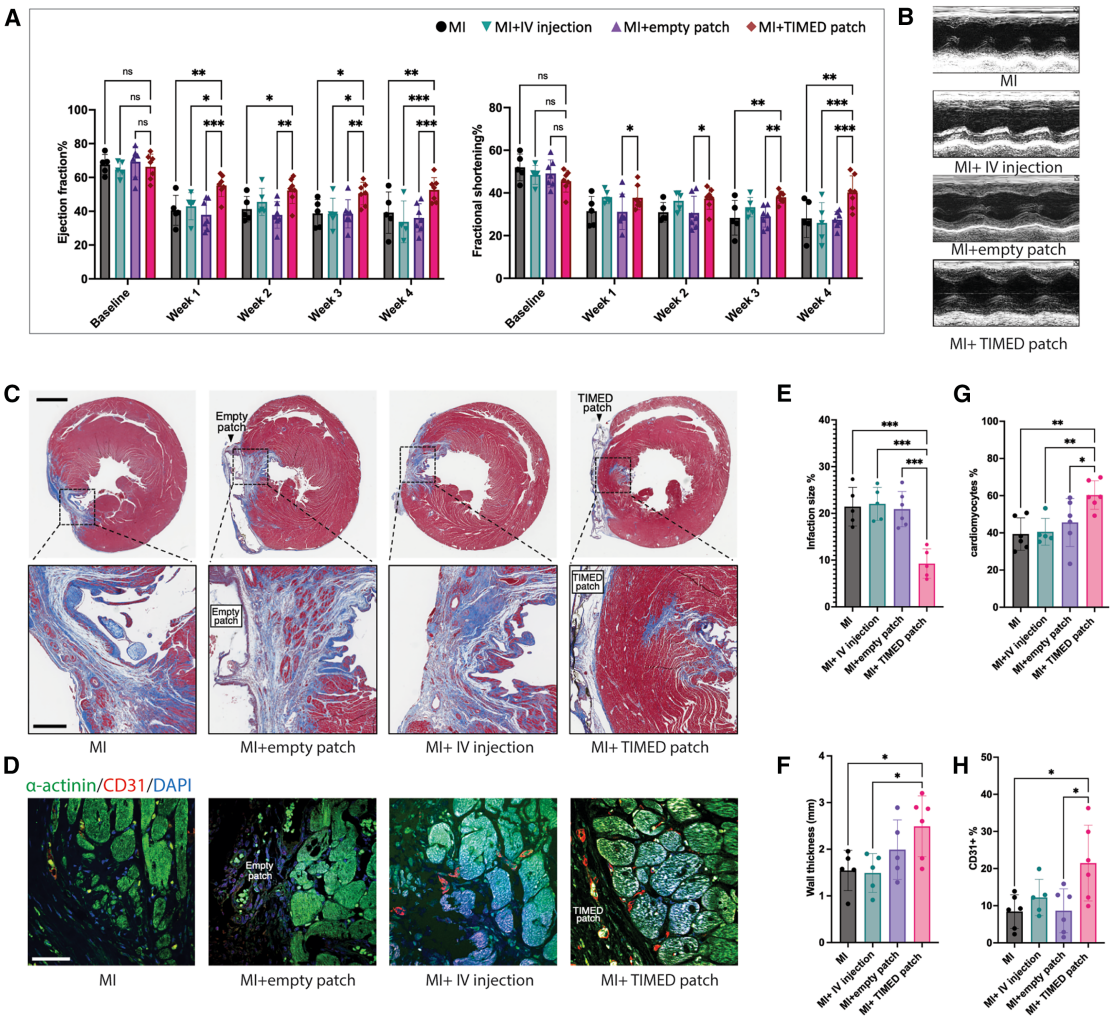

Figure 6. *In vivo* functionality of TIMED patch in rats post MI.

(A) Quantification of ejection fraction and fractional shortening of the heart at corresponding time points for assessing cardiac function over time. $n \geq 5$.

(B) Representative M-mode echocardiography images at endpoint as a visual indicator of cardiac motion.

(C) Representative images of Masson's trichrome staining showing collagen deposition. Scale bar, 2 mm. Infarct zones in the left ventricle are magnified for enhanced visualization. Scale bar, 500 μm.

(D) Representative confocal images of the infarct zone staining with alpha-actinin and CD31. Scale bar, 50 μm.

(E–H) Quantifications of infarct size percentage (E), wall thickness (F), and cardiomyocytes (G) and endothelial cell (H) distribution in the infarct zone. $n \geq 5$. Data represent the mean ± SD. Ordinary one-way ANOVA or ordinary two-way ANOVA (Sidak's multiple comparisons test) were used. p values are represented by $^{*}p \leq 0.05$; $^{**}p \leq 0.01$; $^{***}p \leq 0.001$; $^{****}p \leq 0.000$; ns, not significant.

notable 2.6-fold increase in CD31-positive cells observed in the infarct zone of the TIMED patch group indicates the effective delivery of VEGF, promoting enhanced neovascularization (Figure 6H). These results indicate the patch's capability to mitigate cardiac injury and beneficially modulate cardiac function, emphasizing its effectiveness as a multi-modular delivery system.

To assess degradation kinetics, we quantified patch dry mass before implantation and after 1 month *in vivo*, observing a 20%–30% reduction (Figure S16B). These data indicate that the matrix undergoes gradual resorption, while maintaining structural integrity during the early therapeutic window. Future work will focus on tuning degradation by modifying crosslink density or incorporating cleavable linkers to better match therapeutic release requirements.

DISCUSSION

The TIMED system implements a dual-carrier design strategy engineered to deliver a temporally controlled solution for post-surgical drug delivery, thereby augmenting efficacy and precision in localized drug administration. Within this framework, the tough hydrogel matrix serves as a secondary protective barrier for encapsulated microparticles, enhancing stability against degradation, and ensuring secure immobilization at the surgical site to facilitate sustained therapeutic release. Concurrently, the

Please cite this article in press as: Wang et al., TIMED: Temporal intervention with microparticle encapsulation and delivery—A programmed release system for post-myocardial infarction therapy, Cell Biomaterials (2025), https://doi.org/10.1016/j.celbio.2025.100249

microparticle array offers high encapsulation efficiency and facilitates precise adjustment of initial release times to align with specific therapeutic requirements. By modulating drug-release kinetics to match the dynamic nature of post-operative healing processes, this approach holds the potential to re-imagine treatment outcomes, possibly reducing complications and enhancing long-term recovery.

In cardiac application, the TIMED system modulates drug release to align with the distinct phases of cardiac recovery: neuregulin-1 for immediate protection post MI, VEGF to enhance angiogenesis during recovery, and a TGF-β inhibitor to prevent late-stage fibrosis without disrupting early tissue repair. Delayed administration of neuregulin-1 can miss the critical window for preventing cell death, while early administration of TGF-β inhibitors might interfere with essential collagen buildup for initial recovery. This sequenced pulsatile drug release maximizes the therapeutic benefits of each drug and minimizes adverse effects, such as impaired healing, surpassing the capabilities of monophase delivery systems, such as sustained-release drug patches and injection-based systems.[69–71] These conventional systems lack the ability to provide pulsed timing for different drugs and typically release all drugs simultaneously, which do not match the dynamically changing needs of cardiac recovery, ultimately limiting their effectiveness in complex therapeutic scenarios.

Furthermore, the TIMED patch demonstrated capacity for long-term storage with minimal protein degradation or deterioration in mechanical properties, maintaining stability of the encapsulated drugs above 80% and mechanical strength above 85% of their initial value after 1 month of refrigeration. This stability significantly surpasses emulsion-based systems and other drug-eluting hydrogel systems, some of which exhibit low stability in storage and require to be freshly prepared on site.[69–71] The broad accessibility and simple fabrication of our platform make it an ideal solution across diverse healthcare settings, which could potentially enhance both efficiency and practicality.[72,73] In terms of safety, DSC and fatigue testing confirmed the structural stability of the PLGA caps, and both *in vitro* and *in vivo* profiles showed on-schedule release without leakage. While scaling up production could pose risks of premature release due to fabrication defects, these risks can be mitigated by quality control and sealing strategies, which will be essential for safe clinical translation.

With demonstrated application in both hiPSC-derived cardiac tissues and a rodent model of acute MI, an area where timely intervention is crucial to curtail irreversible cardiac tissue damage, the system holds great potential for combination therapy and adaptability in addressing cardiac repair. In cardiac tissue, the implemented TIMED patch increased cell viability by 1.5-folds relative to hypoxic controls. In the rodent MI model encompassing both male and female cohorts, TIMED patch implantation yielded a 33% augmentation compared with untreated MI and 17% increase compared with i.v. injection in survival rates. This is accompanied by above 15% enhancement in both EF and FS, compared with the MI group and i.v. injection control groups at endpoint. Additionally, an approximate 50% reduction in infarction size was observed, indicating the patch's effectiveness in promoting tissue regeneration and mitigating damage. Functional recovery with the TIMED patch is consistent with outcomes reported for cell-based, EV-loaded, and engineered hydrogel patches in rodent MI models.[74–77] The TIMED patch replicates these benefits through a streamlined acellular approach, in which temporally programmed release of survival, angiogenic, and anti-fibrotic cues produce comparable improvements in systolic function and remodeling. This supports the concept that phase-timed delivery can serve as an effective alternative to more complex strategies involving live cells, with potential advantages for manufacturability, stability, and translational safety.

The patch remains securely in place throughout the implantation process and post-operative period in a highly dynamic environment involving heart contractions, thus ensuring targeted and consistent therapeutic effects with minimal risk of material migration. Additionally, implantation with the TIMED patch demonstrated an unexpected yet significant reduction in surgical adhesion, representing a remarkable 69% reduction compared with the control group, likely, in part, associated with the modulation of TGF-β, which is a potent pathway that regulates collagen synthesis. Collagen has an essential role in early tissue regeneration, but it can lead to fibrous bands or adhesions, particularly during the later repair stages when tissues begin to scar. Releasing a TGF-β inhibitor in week 2 via the TIMED patch curbs this overexpression, ensuring initial collagen deposition, while preventing the excessive buildup that causes adhesions. Furthermore, histological analysis at the patch-epicardium interface revealed denser cellular infiltrates and greater $CD68^+$ macrophage presence in empty patches, whereas TIMED patches showed reduced infiltration and more organized myocardium (Figures S17C and S17D). These findings suggest that local inflammation, together with fibrosis, may shape adhesion outcomes, although time-resolved studies will be needed to more precisely define their interplay. This observation potentially broadens its application to improve post-operative adhesions induced by surgical intervention, and merits more detailed future investigation to explore the anti-adhesion potential of the TIMED patch. This could offer a dual-functional solution, controlling fibrosis and enhancing tissue recovery, making it more versatile than conventional anti-adhesive barrier films or gels that only address physical interactions to avoid adhesions.[78,79] Reduced pericardial adhesions are clinically important, as they complicate re-entry in repeat cardiac surgery. Because adhesion formation is largely confined to the acute post-surgical period and is generally stabilized within the first month, the likelihood of new adhesion formation thereafter is considered low.[79–81] Together with the biocompatibility of the patch, these findings support the long-term translational relevance of this approach.

In conclusion, the collective findings demonstrate the significant potential of the TIMED system in delivering multiple drugs to cardiac tissue at designated time points, aligning intricately with dynamic tissue remodeling including cell survival, angiogenesis, and collagen deposition for cardiac regeneration. This approach enables precision combination therapy, facilitating temporal intervention tailored to specific disease phases related to cardiac tissue post MI.

The modular and adaptable design of the TIMED system extends well beyond the demonstrated treatment regimen. By leveraging a characterized microparticle library, therapeutic

Please cite this article in press as: Wang et al., TIMED: Temporal intervention with microparticle encapsulation and delivery—A programmed release system for post-myocardial infarction therapy, Cell Biomaterials (2025), https://doi.org/10.1016/j.celbio.2025.100249

combinations can be precisely tuned through spatial patterning of MPs, enabling customizable sequential drug release tailored to clinically relevant regimens. The TIMED platform's ability to program multi-phase drug release could optimize treatment protocols and extend to numerous other therapeutic areas, where precisely scheduled interventions improve efficacy and safety. For instance, recent studies highlight the benefits of sequential therapy, such as administering poly(ADP-ribose) polymerase (PARP) inhibitors followed by DNA damage checkpoint inhibitors to enhance tumor cell elimination, while minimizing cytotoxicity.[82]

While this study establishes a framework for controlled, sequential drug release, we acknowledge that surgical implantation may pose challenges for immediate clinical adoption. The system was initially designed for integration into open-chest procedures, such as bypass surgery, where direct implantation is feasible without adding procedural risk, and it can also be adapted for other implantable interventions. This design choice ensures feasibility in current surgical contexts, while providing a foundation for future adaptation. Looking ahead, the clinical utility of the platform can be further expanded through the development of minimally invasive approaches, including catheter-based delivery. The TIMED microparticle array is inherently modular and readily adaptable to such alternative platforms. To further support clinical translation, ongoing studies will focus on optimizing therapeutic pairings, refining release kinetics, and evaluating long-term efficacy. The programmable design of the TIMED system allows incorporation of alternative therapeutic agents and tailored release schedules to better reflect human repair biology and emerging clinical strategies. In addition, we are planning studies in more clinically relevant settings, including IR injury and large-animal models, recognizing that translation to patient application will require a careful, stepwise approach. Collectively, these engineering advancements position TIMED as a scalable and versatile platform, with the potential to transform sequential treatment across a broad spectrum of complex diseases.

METHODS

Microfabrication of drug-loaded PLGA microparticle arrays

SU-8 photoresist and polydimethylsiloxane (PDMS) models were microfabricated using soft lithography techniques as previously described.[28] PLGA powders were purchased from Evonik and PolySciTech. PLGA films were formed using a solvent casting technique.[28] Different PLGA films were then patterned and thermally pressed against PDMS molds at 150°C under vacuum to create microscale PLGA cap and base arrays. The resulting PLGA base arrays were loaded with aqueous solutions, either using an automated picoliter dispensing system (cellenONE, Cellenion) or manually with a 1 μL microliter syringe (Model 7001 KH, Knurled Hub, 25 gauge). The filled base arrays were then thermally bonded to the PLGA cap arrays using a photomask aligner equipped with a Peltier heating element, ensuring precise alignment at the glass transition temperature of PLGA and a secure, accurate bond between the cap and base arrays.

Fabrication of TIMED patch

PLGA microparticle arrays were placed between Fisherbrand glass microslides, separated by 7-mm spacers to maintain uniform thickness, and immersed in a hydrogel precursor solution. This solution consisted of a 10% high MW poly(ethylene glycol) diacrylate (Advanced Biomatrix, MW = 20,000, 50-225-5939), 2.5% alginate (Sigma, A2033), mixed with specified concentrations of calcium sulfate and a photoinitiator (Irgacure 2959, Sigma). The assembly was then exposed to UV light for 30 s in a UV chamber (Fisherbrand, 254 nm, 80 W) to initiate hydrogel crosslinking. After curing, the crosslinked hydrogel-embedded patch was carefully detached from the bottom glass slide using a razor blade and inverted. An additional hydrogel layer was then applied using 3-mm spacers to ensure the MP arrays were securely embedded within the hydrogel matrix through covalent bonds with the first layer. Following fabrication, patches were hydrated by applying sterile saline to the surface and placed in sealed, humidified tubes for ~1 h to reach a swollen state prior to implantation and mechanical tests. This procedure maintained hydration and mechanical stability, while avoiding prolonged buffer incubation that could accelerate PLGA degradation.

Measurement of tensile strength and elasticity of hydrogel patch

The Young's modulus of a hydrogel patch is measured through tensile testing by clamping the hydrogel sample between the grips of a tensile testing machine (Instron, Model 5543, the loading cell is 250 N), and elongating it at a constant rate (200% min^{-1}) until failure. During the test, the force applied to the sample and the corresponding elongation are recorded. The tensile strain (ε) was defined as the length change (Δl) divided by the original length (l_0) of the sample. Young's modulus was calculated from the linear region of the strain-stress curve. To simulate long-term cardiac application, a testing method was developed using a balloon system actuated by a positive pressure ventilator. The balloon's volume was set to approximately 0.5 mL, with the TIMED patch affixed to the balloon surface. This setup was placed within a flask filled with media at 37°C. Utilizing a ventilator (Kent Scientifics, RoVent Jr. Small Animal Ventilator), the system induced the balloon's expansion and contraction at a heart rate of 300 bpm and a tidal volume of 3 mL. This regimen subjected the hydrogel patch to 2 million cycles of stretching, akin to the heart's movements over the course of approximately 1 month. Following the stretching, the Young's modulus of the hydrogel patch was evaluated to determine its mechanical integrity post simulation.

Differential scanning calorimetry (DSC) measurements

DSC analysis was performed on various samples, including polymer powder, microparticles both before and after sealing, empty patches, and TIMED patches, as previously reported.[83] The samples (between 1–20 mg) were placed into aluminum Tzero Pan (TA Instruments, 901683.901). Pans were sealed using Tzero Lid (TA Instruments, 901671.901). The thermal behavior of the materials was analyzed using a TA Instruments Discovery DSC 25, with thermograms recorded over a temperature range of 10°C to 100°C at a heating rate of 10°C/min. The glass

transition temperature of the samples was determined using the TA Instruments DSC TRIOS v.5.7.2.101 software, peak temperature values were reported as the glass transition temperatures.

Swelling ratio and degradation rate of the hydrogel patch

The swelling ratio and degradation rate of the hydrogel component were analyzed subsequent to hydrogel fabrication in different conditions. Hydrogel patches were immersed in distilled water, phosphate-buffered saline (PBS, pH = 7.4, Gibco, 10010049), and saline solution (Alkali Scientific, DS0329). These patches were placed in an incubator maintained at 37°C. The dynamic water uptake of the hydrogels was evaluated at predetermined intervals by measuring the hydrogel's weight post immersion. Excess surface moisture was removed with filter paper prior to weighing. The degree of swelling was expressed as a percentage, representing the increase in weight due to water absorption compared with the original weight of the hydrogel. The degradation rate of the hydrogel in a timed-release application was assessed by immersing the patches in PBS and cell culture media at 37°C. After specific time intervals, each patch was lyophilized and then weighed. The initial dry weight and the post-incubation dry weight at each interval were recorded to evaluate the percentage of material degraded over time.

Biocompatibility and toxicity

Cytotoxicity assays using HUVECs (PromoCell, C-12203) assessed the patch's biocompatibility, comparing it against PAAM hydrogel controls (acrylamide, Sigma, A8887). Initially, 50,000 cells were seeded in each well of a 24-well plate. Upon reaching confluence, the TIMED patch and PAAM patch were placed in Corning transwell polycarbonate membrane cell culture inserts (CLS3402), along with empty controls, above the cell layer for a period of 4 days. Cell viability was assessed with a live/dead viability/cytotoxicity (Invitrogen, L3224) assay and imaged under a DeltaVision Ultra microscope.

Simulation and screening of drug-release kinetics

For computational simulations, COMSOL Multiphysics 5.3 (Stockholm, Sweden) was used. For the hydrogel, a linear elastic model was applied with Young's modulus (E) of 1,000 Pa, Poisson's ratio (Υ) of 0.4, and a density (ρ) of 1 g/cm^3. For the microparticles, the linear elastic model was applied with an E of 20, 7, and 5 MPa for low, medium, and high MW PLGAs, respectively, as higher MW PLGA exhibits lower E. As standard PLGAs, Υ of 0.3, ρ of 1.34 g/cm^3, permeability of 1e−7 m^2, and porosity of 0.1 were used. Darcy's law was applied for fluid interaction. For fluid, standard water was used with ρ of 1 g/cm^3 and viscosity (μ) of 8.9e−4 Pa*s. Inlet and outlet velocities were fixed to 1e−5 m/s. Inlet and outlet pressures were fixed to 101,325 Pa and 0 Pa, respectively. The simulations were run at 1 atm environment with a Biot-Willis coefficient of 1.

In vitro validation of drug-release kinetics

In vitro validation of drug-release kinetics was performed using TIMED patches loaded with fluorescent dye-conjugated dextran (10 kDa; Biotium, cat. 80110–80118) encapsulated within the microparticles. Release profiles were quantified to assess *in vitro* drug release from the patches. Each patch was then positioned on a 12-well transwell insert (Corning, CLS3402), with a release buffer containing 0.5% BSA (Sigma-Aldrich, A7030) in PBS situated beneath the insert, to simulate physiological conditions. This assembly was incubated at a constant temperature of 37°C to mimic the human body's internal environment. At predetermined time points, samples of the release buffer were collected and analyzed using a plate reader (Tecan Plate Reader Infinite F200) to quantitatively measure the concentration of the fluorescently labeled dextran.

Release kinetics under *in vitro* stretch simulation

To evaluate the effect of mechanical strain on drug release, a stretchable PDMS membrane was bonded to a bottomless 6-well plate (CSCSM0061, CS CRIE), creating a sealed chamber. The TIMED patch was anchored to the membrane in an open well, while the remaining wells were sealed with airtight covers using 3D-printed frames and gaskets (OrganoBiotech). The open well was connected to a RoVent Jr. Small Animal Ventilator, delivering 3 mL per actuation at 300 bpm to simulate rat heart contractions. The system was maintained at 37°C, and 1 mL of release buffer was collected at defined intervals for analysis. This setup enabled the assessment of release kinetics under physiologically relevant cyclic strain.

Liquid chromatography–mass spectrometry (LC–MS)

LC-MS was performed to identify and quantify GW 788388 loaded in the patch. An Agilent 6125B mass spectrometer attached to an Agilent 1260 Infinity LC was used with a C-18 column. An electrospray (ESI) source was equipped, and the diode array has a wavelength range of 190–640 nm, and a measurable m/z range of 100–1,500 Da. The mobile phase consisted of water and acetonitrile. A gradient elution program was employed with the following profile: 0–1 min 10% B, 1–5 min 10%–100% B. An extracted ion chromatogram (EIC) feature was applied for characterizations of the molecule.

Generation and assessment of cardiac spheres

Cardiac spheroids were generated by combining 60% iCell cardiomyocytes (Cellular Dynamics, 01434 -R1057) with 20% human cardiac fibroblasts (Lonza, CC-2904) and 20% HUVECs (PromoCell,C-12203) in a customized media. This media was a blend of iCell cardiomyocytes maintenance medium (Celluar Dynamics, M1003), endothelial cell growth medium 2 (Sigma-Aldrich, C-22011), and fibroblast growth medium 3 (Sigma-Aldrich, C-23130) in a 1:1:1 ratio. Spheroid formation occurred through self-assembly on Corning Ultra-Low Attachment Surface plates (Corning, 4515). Tissue compaction was observed by day 3, at which point a hypoxic environment was induced using an incubator set to 1% oxygen for 24 h to simulate hypoxic conditions. The spheroids were transferred to the bottom of the well plate, and the drug-loaded timed-release patch was positioned on the insert above them for incubation over the course of 3 weeks. Upon endpoint, after removing media, the spheres are washed with PBS and viability was assessed with a live/dead viability/cytotoxicity (Invitrogen, L3224) assay. For immunostaining, the spheres were fixed with 4% paraformaldehyde,

Please cite this article in press as: Wang et al., TIMED: Temporal intervention with microparticle encapsulation and delivery—A programmed release system for post-myocardial infarction therapy, Cell Biomaterials (2025), https://doi.org/10.1016/j.celbio.2025.100249

permeabilized by 0.25% Triton X-100, and blocked by 5% BSA. Immunostaining was performed as previously described,[84] using the antibodies including rabbit anti-α-actinin (Abcam, ab137346; 1:200), mouse anti-CD31 (Novus Biologicals NB10064796T, 1:200), mouse anti-type I collagen (GeneTex GTX26308, 1:200), and the secondary antibodies donkey anti-mouse Alexa Fluor 488 (Abcam ab150105; 1:500) and donkey anti-rabbit Alexa Fluor 594 (Life Technologies A-21207; 1:1000). Confocal microscopy images were obtained using an Olympus FluoView 1200 laser scanning confocal microscope (Olympus Corporation).

Surgical ligation of the LAD artery in rats

All animal procedures received approval from the Massachusetts Institute of Technology Committee on Animal Care (2304000509) and were overseen by the Division of Comparative Medicine (DCM) in an Association for Assessment and Accreditation of Laboratory Animal Care International (AAALAC) accredited facility.

Wistar rats aged 5 to 9 months from Charles River Laboratories were sex-matched in each experimental group. Prior to surgery, rats were pre-medicated with buprenorphine-extended-release (0.9 mg/kg subcutaneous) and sedated with ketamine and xylazine (70 mg/kg intraperitoneal). They were then intubated, placed supine on a heated pad, and ventilated with a RoVent Jr. Small Animal Ventilator. Appropriate tidal volume and respiratory rate were set based on weight, eyes were lubricated, and limbs secured. The inspiratory-to-expiratory ratio was set to 1:1 to prevent pulmonary atelectasis. The surgical site was prepped aseptically, and a left anterolateral intercoastal incision was made above the xiphoid, penetrating down to the pleura, following infiltration of bupivacaine into the muscle layers. After blunt entry into the chest cavity, the left lateral aspect of the heart was exposed using retractors, and the LAD artery was ligated with a 6-0 (Ethicon Prolene) stitch. The chest was closed in layers, and negative pressure was applied to ensure no air remained in the chest cavity before sealing. Xylazine was reversed with atipamezole (70 mg/kg, half intraperitoneally and half subcutaneously) after thoracic closure and before recovery.

Implantation of TIMED patch following MI induction

For rats in which a patch was placed, the procedure proceeded as described above, following LAD ligation. Directly after ligation, three stitches were placed in the superficial myocardium to anchor the patch—two at the level of the ligation stitch, one medial and one lateral to the ligation stitch, and one at the apex of the heart. The stitches at the level of the ligation stitch were spaced to match approximately the width of the patch, using 7-0 (DemeSILK) or 8-0 (Ethicon Prolene) sutures. The needles were then passed through the patch and tied down. Each stitch was tied with 5–7 throws. The chest was then closed as described above. For all medicated patches, microparticles were nanodispensed with 1 μg of the corresponding compound, including human NRG1 (RHNRG1/HRG1 CF, 5898NR050, Fisher Scientific), human VEGF165 (RVEGFI, Invitrogen), or GW788388 (502173102, Fisher Scientific), along with excipients, in three distinct sections of the microparticle arrays. Three distinct microparticle sets were sealed with PLGA caps of different formulations to program staggered release. The assembled microparticle array was then encapsulated within a PEGDA/alginate hydrogel to form the complete patch. For implantation, the NRG1-loaded microparticle side was oriented toward the lateral epicardial surface to ensure consistent placement across experiments. The chest was closed in layers, ensuring no air remained in the chest cavity before sealing.

I.v. tail vein injections of soluble controls

To provide a systemic comparator for the TIMED patch, i.v. tail vein injections were performed on days 1, 7, and 14 post MI, corresponding to the three programmed release events of the patch. Each injection contained 1 μg of each therapeutic agent (NRG1, VEGF, and GW788388), matching the mass of each pulse released from the TIMED patch. The therapeutics were dissolved as solutions in sterile 0.9% saline without excipients, to contrast systemic bolus delivery with localized encapsulated release. Injections were administered in a total volume of 200 μL via the tail vein using a 24 G needle under light isoflurane anesthesia.

Blood sample collection from lateral tail vein

The animals were placed under isoflurane anesthesia, and blood samples were obtained from the lateral tail vein using a 24 G Surflo IV catheter. Blood was collected via capillary action into a serum-separating tube. The serum was subsequently obtained by centrifuging at 10,000 rpm for 3 min at 4°C. The serum was then stored in a −20°C freezer upon analysis.

Blood sample concentration for *in vivo* release kinetics study

Rat serum samples were first concentrated using Amicon Ultra 0.5 mL centrifugal filters with a 30 kDa MW cutoff (MilliporeSigma, Burlington, MA, USA) for human VEGF165 and human NRG1/HRG1. This selection ensures optimal retention of the target proteins while removing lower-MW contaminants. For GW788388, flow-through fractions were collected using Amicon Ultra 10 kDa molecular weight cut-off (MWCO) filters to separate the free drug from protein-bound components. The concentration process was performed according to the manufacturer's instructions by centrifuging the samples at 18,000 × *g* for 20 min at 4°C, ensuring optimal recovery while minimizing sample loss. After concentration, the retained fractions for VEGF165 and NRG1 were carefully transferred to fresh tubes and stored on ice until further processing. ELISA was performed using a Human NRG1 ELISA Kit (Abnova KA4504) and Human VEGF-165 ELISA Kit (ab273164, Abcam), following the manufacturer's protocol. Absorbance was measured at 450 nm using an Infinite M Plex TECAN plate reader, and final concentrations were determined using a standard curve. Additionally, flow-through fractions from the 10 kDa MWCO filters were used for LC-MS analysis to quantify GW788388.

Bioactivity assays for NRG1, VEGF, and GW788388

The functional activity of NRG1 was assessed using MCF-7 cell proliferation. MCF-7 human caucasian breast adenocarcinoma cells (Sigma-Aldrich, 86012803-1VL) were thawed, plated in 96-well plates, and treated with serial dilutions of recombinant

Please cite this article in press as: Wang et al., TIMED: Temporal intervention with microparticle encapsulation and delivery—A programmed release system for post-myocardial infarction therapy, Cell Biomaterials (2025), https://doi.org/10.1016/j.celbio.2025.100249

human NRG1 or NRG1 samples from various experimental conditions (filtered through a sterile syringe filter). After 72 h, cell proliferation was quantified using the CellTiter-Glo Luminescent Cell Viability Assay (TECAN Infinite M Plex). Bioactivity was determined by plotting a dose-response curve.

The ability of VEGF to activate VEGFR2 signaling was evaluated using the VEGF Reporter Bioassay (Promega, GA2001). VEGFR2 reporter cells (2×10^5 cells/well) were plated in 96-well plates and treated with 100 μL of stored VEGF release buffer from various conditions, alongside standard curve dilutions. ONE-Glo Luciferase Reagent was added, and luminescence was measured using the TECAN Infinite M Plex. VEGF bioactivity was quantified by plotting relative luminescence units (RLU) against a standard curve.

GW788388 activity was assessed by its ability to inhibit TGF-β signaling using HEK-BLUE TGF-β Reporter Cells (InvivoGen, HKB-TGFBv2). Cells were plated in 96-well plates and stimulated with TGF-β1 (2 ng/mL, Sigma-Aldrich, H8541) as a positive control for pathway activation. Supernatants containing GW788388 from various experimental conditions were added alongside standard curve dilutions, and the assay was incubated for 24 h. Secreted embryonic alkaline phosphatase (SEAP) activity was measured at 620–655 nm using the TECAN Infinite M Plex. A reduction in SEAP activity indicated effective TGF-β inhibition, with bioactivity quantified against a standard curve.

RT-qPCR

Total RNA was collected using RNeasy Plus Micro Kit (QIAGEN 74134) following the manufacturer's instructions. cDNAs were synthesized by reverse transcription (RT) using qScript cDNA Supermix (QuantaBio 95048–500). RT-qPCR was carried out using Fast SYBR Green Master Mix (Thermo Fisher 4385618) and recorded on a Thermo Fisher Scientific QuantStudio 6 machine. Glyceraldehyde-3-phosphate dehydrogenase (GAPDH) was used as the reference gene for the normalization of target gene expression with the 2-ΔCT method. Primer pairs against TNNT2 (PMID: 32627044), GAPDH (PMID: 37741987), BNP (PMID: 37165917), VEGF (PMID: 23935865), PECAM-1 (PMID: 22042082), COL1A1 (PMID: 17576241), TGF-β (PMID: 22042082), MMP2 (PMID: 25013467), caspase-3 (PMID: 11221855), and HIF-1α (PMID: 25013467) were validated in previous studies. Primers for RT-qPCR are listed below:

TNNT2 for, ATGTCTGACATAGAAGAGGTGGTGG
TNNT2 rev, CTATTTCCAGCGCCCGGTGACTTTA
BNP_for, TCTGGCTGCTTTGGGAGGAAGA
BNP_rev, CCTTGTGGAATCAGAAGCAGGTG
VEGF_for, GAGCAAGACAAGAAAATCCC
VEGF_rev, CCTCGGCTTGTCACATCTG
PECAM-1_for, CCAGTGTCCCCAGAAGCAAA
PECAM-1_rev, TGATAACCACTGCAATAAGTCCTTTC
COL1A1_for, GCTTCACCTACAGCGTCACTGTCG
COL1A1_rev, AGAGGAGTTTACAGGAAGCAGACAG
TGF-β_for, GGGAACACCACCACTCTCATTAG
TGF-β_rev, CAAATTACCACTCGGAAGTTCGT
MMP2_for, GGAATGCCATCCCCGATAAC
MMP2_rev, CAGCCTAGCCAGCCAGTCGGATTT
Caspase-3_for, TTCAGAGGGGATCGTTGTAGAAGTC
Caspase-3_rev, CAAGCTTGTCGGCATACTGTTTCAG
HIF-1α_for, TGAAGTGTACCCTACCCTAACTAGCCG
HIF-1α_rev, AATCAGCACCAAGCAGGTCATAG
GAPDH_for, AGAAGGCTGGGGCTCATTTG
GAPDH_rev, AGGGGCCATCCACAGTCTTC

IVIS for biodistribution

Biodistribution studies of compounds encapsulated in the TIMED system were performed using an IVIS (PerkinElmer, Hopkinton, MA, USA). Flamma 774-conjugated dextran (10 kDa; DiagnoCine Lab, RSC0314) was encapsulated within the microparticles of the TIMED patch and implanted onto the rat heart, with an empty patch serving as a negative control. Following the expected release period, rats were euthanized, and major organs, including the heart, lungs, kidneys, liver, and spleen, were collected. Fluorescence imaging was performed using the IVIS system to detect the distribution of Flamma 774, assessing localized retention and systemic biodistribution of the released compounds.

In vivo degradation study

To assess the degradation kinetics of the TIMED patch, total dry mass was measured before implantation and after 1 month *in vivo*. Following euthanasia at the 1-month endpoint, the chest cavity was reopened, and the implanted patch was carefully excised. Adherent tissues were gently removed from the epicardial surface, and residual collagen was enzymatically digested using collagenase type II in PBS, 37°C for 10 min to ensure accurate mass measurements. The patch was then lyophilized to eliminate residual moisture before determining its final dry mass. The percentage of mass loss was calculated relative to the initial dry weight to quantify degradation.

Cardiac injury marker measurement

Serum samples collected at baseline before surgery and at multiple time points post surgery, including day 1, day 3, and weekly until the 4-week endpoint, were diluted and analyzed with the MILLIPLEX MAP Rat Cardiac Injury Panel 1—Cardiotoxicity Multiplex Assay (Millipore, RCI1MAG-87K), configured to measure three markers: troponin I, troponin T, and CK-MB. The assay plate was read using the Bio-Plex 3D suspension array system (Bio-Rad), with data acquisition performed by Luminex xPONENT software.

Echocardiography recording and assessment

Echocardiography was performed at baseline before surgery, and then at the end of weeks 1, 2, 3, and 4 post surgery for all groups. Fine 30 G stainless-steel solid needle electrodes were plugged into a signal transducing box and positioned in the subcutaneous space of the animals' limbs and used to transmit the electrocardiogram (ECG) to the photoacoustic equipment. The data were captured using a Vevo 2100 ultrasound machine and an MX201 transducer probe. During imaging, the animals were under 2% isoflurane anesthesia. The transducer was placed directly on the shaved chest wall. By aligning the transducer along the long axis of the left ventricle (LV) and directing it toward the right side of the neck, a two-dimensional long-axis view of the LV was obtained. The transducer was then

rotated clockwise by 90° to visualize the short-axis view of the LV. The data were analyzed using Visualsonics software (VevoLAB). Measurements of EF were derived from B-mode images obtained via a parasternal long-axis view. FS measurements were conducted using M-mode through a parasternal short-axis view of the heart at the mid-ventricular level.

Histology and immunostaining

At the 4-week time point, hearts were extracted from the chest cavity. Potassium chloride solution was perfused through the aorta using a 5 mL syringe and a feeding needle secured with 4-0 suture to induce relaxation of the heart muscle. Following this, the atrium was carefully incised to allow the formalin solution to be perfused into the hearts under fixed pressure, ensuring uniform distribution throughout the tissue. The hearts were then immersed in formalin for 48 h to achieve complete fixation before undergoing paraffin embedding. Histological analysis involved obtaining sections from the area just below the LAD ligation point, with additional sections taken at 250-micron intervals. Samples were then wax embedded and sectioned into 5-μm slices using a microtome and mounted onto glass slides for staining with H&E and Masson's trichrome to assess tissue morphology and collagen deposition, respectively. For antigen retrieval, sections were deparaffinized, rehydrated, and placed in a pressure cooker set to high pressure and heated for 20 min with antigen retrieval buffer (Abcam, ab93684). Immunostaining was performed using the primary antibodies including rabbit anti-α-actinin, mouse anti-CD31, and the secondary antibodies donkey anti-mouse Alexa Fluor 488 and donkey anti-rabbit Alexa Fluor 594. To assess myocardial delivery, TIMED patches were loaded with Texas Red-conjugated dextran (40 kDa; Invitrogen, D1829), and tissue was co-stained with α-actinin to visualize molecular diffusion within cardiac tissue. Confocal microscopy images were obtained using an Olympus FluoView 1200 laser scanning confocal microscope (Olympus Corporation).

Statistical analysis

All *in vitro* experiments were performed in experimental triplicate or quintuplicate unless noted otherwise. All *in vivo* experiments were designed to include at least six experimental replicates in each group. Assessments at different time points were conducted with all available animals due to variability in survival rates. Statistical analyses were performed using GraphPad Prism software. Differences between experimental groups were analyzed by Student's *t* test (two groups), one-way ANOVA (more than two groups), or two-way ANOVA (two different variables). The normality test (Shapiro-Wilk) and pairwise multiple comparison procedures (Tukey's post hoc method or Holm-Sidak method) were used for one-way and two-way ANOVA tests. p values are represented by $^{*}p \leq 0.05$; $^{**}p \leq 0.01$; $^{***}p \leq 0.001$; $^{****}p \leq 0.0001$.

RESOURCE AVAILABILITY

Lead contact

Requests for further information and resources should be directed to and will be fulfilled by the lead contact, Ana Jaklenec (jaklenec@mit.edu).

Materials availability

All reagents and materials supporting the findings of this study are available and will be freely distributed from the corresponding authors upon request.

Data and code availability

All data associated with this study are present in the paper or supplemental materials. Any additional information required to reanalyze the data reported in this paper will be available from the lead contact upon request.

ACKNOWLEDGMENTS

We thank the Koch Institute's Robert A. Swanson (1969) Biotechnology Center (RRID: SCR_018674) for technical support, specifically the Histology core, the Nanotechnology Materials core, and the Animal Imaging and Preclinical Testing facilities. Special thanks go to Dr. Giovanni Traverso for providing instruments for hydrogel fabrication, and Dr. J. Christopher Love and Joshua Hinckley for assistance with the Luminex assay. We acknowledge the MIT animal facilities for guiding our *in vivo* studies, especially to Wontaek Chung and Emily Franklin for providing supervision to our surgical procedures, and Nicole Henning for assisting with ultrasound analysis. E.Y.W. and B.Y. are supported by Banting Postdoctoral Fellowship sponsored by the Natural Sciences and Engineering Research Council of Canada (NSERC), and the Government of Canada. E.A.C. was supported by an NHLBI Career Development Award in Translational Glycobiology (NIH 5K12HL141953-02) and acknowledges the collaborative opportunities from the MIT Convergence Scholars Program and academic development time from the MGH Department of Surgery. We thank Sydney MacDonald for her administrative support, and Dhruv Varshney, Audrey McCarthy, and Mehr Chaddah for their technical assistance.

AUTHOR CONTRIBUTIONS

Conceptualization, E.Y.W. and A.J.; methodology, E.Y.W., E.A.C., B.Y., A.G.B., and B.E.; investigation, E.Y.W., E.A.C., B.Y., B.E., L.Z., A.G.B., J.H., X.Y., Y.H., C.J.Q., and Y.L.; visualization, E.Y.W., B.E., J.H., and X.Y.; funding acquisition, A.J. and R.L.; project administration, E.Y.W. and A.J.; supervision, E.Y.W., R.L., and A.J.; writing—original draft, E.Y.W,; writing—review & editing, E.Y.W., E.A.C., A.G.B., B.Y., B.E., R.L,. A.J.

DECLARATION OF INTERESTS

From FY 2020 to the present, A.J. receives licensing fees (to patents on which she was an inventor) from, invested in, consults (or was on Scientific Advisory Boards or Boards of Directors) for, lectured (and received a fee), or conducts sponsored research at MIT for which she was not paid for the following entities: The Estée Lauder Companies, Moderna Therapeutics, OmniPulse Biosciences, Particles for Humanity, SiO2 Materials Science, and VitaKey.

From FY 2021 to the present, R.L. receives licensing fees (to patents in which he was an inventor on) from, invested in, consults (or was on Scientific Advisory Boards or Boards of Directors) for, lectured (and received a fee), or conducts sponsored research at MIT for which he was not paid for the following entities: https://www.dropbox.com/scl/fo/9hrpxuzs72iwvmoqze7rx/AA_OoThWVjAex7X_LhwLRcw?rlkey=llza5qcutubtyx34uqrrfy141&st=zcgqc4qp&dl=0

SUPPLEMENTAL INFORMATION

Supplemental information can be found online at https://doi.org/10.1016/j.celbio.2025.100249.

Received: June 9, 2025
Revised: September 9, 2025
Accepted: October 8, 2025

REFERENCES

1. Roth, G.A., Mensah, G.A., Johnson, C.O., Addolorato, G., Ammirati, E., Baddour, L.M., Barengo, N.C., Beaton, A.Z., Benjamin, E.J., Benziger, C.P., et al. (2020). Global Burden of Cardiovascular Diseases and Risk Factors, 1990–2019: Update From the GBD 2019 Study. J. Am. Coll. Cardiol. *76*, 2982–3021. https://doi.org/10.1016/j.jacc.2020.11.010.
2. Manfroi, W.C., Peukert, C., Berti, C.B., Noer, C., Gutierres, Dde A., and Silva, F.T. (2002). Acute myocardial infarction: the first manifestation of ischemic heart disease and relation to risk factors. Arq. Bras. Cardiol. *78*, 392–395. https://doi.org/10.1590/s0066-782x2002000400006.
3. Kumphune, S., Piot, C., and Barrere-Lemaire, S. (2023). Editorial: New strategies to inhibit cell death in myocardial ischemia-reperfusion injury: how to succeed? Volume II. Front. Cardiovasc. Med. *10*, 1260800. https://doi.org/10.3389/fcvm.2023.1260800.
4. Jia, X.F., Liang, F.G., and Kitsis, R.N. (2021). Multiple Cell Death Programs Contribute to Myocardial Infarction. Circ. Res. *129*, 397–399. https://doi.org/10.1161/CIRCRESAHA.121.319584.
5. Ríos-Navarro, C., Gavara, J., Núñez, J., Revuelta-López, E., Monmeneu, J.V., López-Lereu, M.P., de Dios, E., Pérez-Solé, N., Vila, J.M., Oltra, R., et al. (2022). EpCAM and microvascular obstruction in patients with STEMI: a cardiac magnetic resonance study. Rev. Esp. Cardiol. (Engl Ed) *75*, 384–391. https://doi.org/10.1016/j.rec.2021.04.006.
6. Wang, E.Y., Rafatian, N., Zhao, Y., Lee, A., Lai, B.F.L., Lu, R.X., Jekic, D., Davenport Huyer, L., Knee-Walden, E.J., Bhattacharya, S., et al. (2019). Biowire Model of Interstitial and Focal Cardiac Fibrosis. ACS Cent. Sci. *5*, 1146–1158. https://doi.org/10.1021/acscentsci.9b00052.
7. Singh, K.P., and Harrington, R.A. (2007). Primary percutaneous coronary intervention in acute myocardial infarction. Med. Clin. North Am. *91*, 639–655, x; x-xi.. https://doi.org/10.1016/j.mcna.2007.03.008
8. Fröhlich, G.M., Meier, P., White, S.K., Yellon, D.M., and Hausenloy, D.J. (2013). Myocardial reperfusion injury: looking beyond primary PCI. Eur. Heart J. *34*, 1714–1722. https://doi.org/10.1093/eurheartj/eht090.
9. Kulik, A. (2016). Secondary prevention after coronary artery bypass graft surgery: a primer. Curr. Opin. Cardiol. *31*, 635–643. https://doi.org/10.1097/HCO.0000000000000331.
10. Hannan, E.L., Racz, M.J., Walford, G., Jones, R.H., Ryan, T.J., Bennett, E., Culliford, A.T., Isom, O.W., Gold, J.P., and Rose, E.A. (2005). Long-term outcomes of coronary-artery bypass grafting versus stent implantation. N. Engl. J. Med. *352*, 2174–2183. https://doi.org/10.1056/NEJMoa040316.
11. Cowper, P.A., Knight, J.D., Davidson-Ray, L., Peterson, E.D., Wang, T.Y., and Mark, D.B.; TRANSLATE-ACS Investigators (2019). Acute and 1-Year Hospitalization Costs for Acute Myocardial Infarction Treated With Percutaneous Coronary Intervention: Results From the TRANSLATE-ACS Registry. J. Am. Heart Assoc. *8*, e011322. https://doi.org/10.1161/JAHA.118.011322.
12. Shazly, T., Smith, A., Uline, M.J., and Spinale, F.G. (2022). Therapeutic payload delivery to the myocardium: Evolving strategies and obstacles. JTCVS Open *10*, 185–194. https://doi.org/10.1016/j.xjon.2022.04.043.
13. Wang, E.Y., Zhao, Y., Okhovatian, S., Smith, J.B., and Radisic, M. (2022). Intersection of stem cell biology and engineering towards next generation in vitro models of human fibrosis. Front. Bioeng. Biotechnol. *10*, 1005051. https://doi.org/10.3389/fbioe.2022.1005051.
14. Hu, Y., Zhang, W., Ali, S.R., Takeda, K., Vahl, T.P., Zhu, D., Hong, Y., and Cheng, K. (2025). Extracellular vesicle therapeutics for cardiac repair. J. Mol. Cell. Cardiol. *199*, 12–32. https://doi.org/10.1016/j.yjmcc.2024.11.005.
15. Sahoo, S., Kariya, T., and Ishikawa, K. (2021). Targeted delivery of therapeutic agents to the heart. Nat. Rev. Cardiol. *18*, 389–399. https://doi.org/10.1038/s41569-020-00499-9.
16. Rodness, J., Mihic, A., Miyagi, Y., Wu, J., Weisel, R.D., and Li, R.-K. (2016). VEGF-loaded microsphere patch for local protein delivery to the ischemic heart. Acta Biomater. *45*, 169–181. https://doi.org/10.1016/j.actbio.2016.09.009.
17. Johnson, N.R., Kruger, M., Goetsch, K.P., Zilla, P., Bezuidenhout, D., Wang, Y., and Davies, N.H. (2015). Coacervate Delivery of Growth Factors Combined with a Degradable Hydrogel Preserves Heart Function after Myocardial Infarction. ACS Biomater. Sci. Eng. *1*, 753–759. https://doi.org/10.1021/acsbiomaterials.5b00077.
18. Chen, H., Fan, L., Peng, N., Yin, Y., Mu, D., Wang, J., Meng, R., and Xie, J. (2022). Galunisertib-Loaded Gelatin Methacryloyl Hydrogel Microneedle Patch for Cardiac Repair after Myocardial Infarction. ACS Appl. Mater. Interfaces *14*, 40491–40500. https://doi.org/10.1021/acsami.2c05352.
19. Oliva, N., Conde, J., Wang, K., and Artzi, N. (2017). Designing Hydrogels for On-Demand Therapy. Acc. Chem. Res. *50*, 669–679. https://doi.org/10.1021/acs.accounts.6b00536.
20. Li, J., and Mooney, D.J. (2016). Designing hydrogels for controlled drug delivery. Nat. Rev. Mater. *1*, 16071. https://doi.org/10.1038/natrevmats.2016.71.
21. Ahmed, E.M. (2015). Hydrogel: Preparation, characterization, and applications: A review. J. Adv. Res. *6*, 105–121. https://doi.org/10.1016/j.jare.2013.07.006.
22. Yong, J., Tao, J., Wang, K., Li, X., and Yang, Y. (2025). Post-myocardial Infarction Cardiac Remodeling: Multidimensional Mechanisms and Clinical Prospects of Stem Cell Therapy. Stem Cell Rev. Rep. *21*, 1369–1427. https://doi.org/10.1007/s12015-025-10888-7.
23. Ferrini, A., Stevens, M.M., Sattler, S., and Rosenthal, N. (2019). Toward Regeneration of the Heart: Bioengineering Strategies for Immunomodulation. Front. Cardiovasc. Med. *6*, 26. https://doi.org/10.3389/fcvm.2019.00026.
24. Prabhu, S.D., and Frangogiannis, N.G. (2016). The Biological Basis for Cardiac Repair After Myocardial Infarction: From Inflammation to Fibrosis. Circ. Res. *119*, 91–112. https://doi.org/10.1161/CIRCRESAHA.116.303577.
25. Makadia, H.K., and Siegel, S.J. (2011). Poly Lactic-co-Glycolic Acid (PLGA) as Biodegradable Controlled Drug Delivery Carrier. Polymers (Basel) *3*, 1377–1397. https://doi.org/10.3390/polym3031377.
26. Eldeeb, A.E., Salah, S., and Elkasabgy, N.A. (2022). Biomaterials for Tissue Engineering Applications and Current Updates in the Field: A Comprehensive Review. AAPS PharmSciTech *23*, 267. https://doi.org/10.1208/s12249-022-02419-1.
27. Lu, X., Miao, L., Gao, W., Chen, Z., McHugh, K.J., Sun, Y., Tochka, Z., Tomasic, S., Sadtler, K., Hyacinthe, A., et al. (2020). Engineered PLGA microparticles for long-term, pulsatile release of STING agonist for cancer immunotherapy. Sci. Transl. Med. *12*, eaaz6606. https://doi.org/10.1126/scitranslmed.aaz6606.
28. McHugh, K.J., Nguyen, T.D., Linehan, A.R., Yang, D., Behrens, A.M., Rose, S., Tochka, Z.L., Tzeng, S.Y., Norman, J.J., Anselmo, A.C., et al. (2017). Fabrication of fillable microparticles and other complex 3D microstructures. Science *357*, 1138–1142. https://doi.org/10.1126/science.aaf7447.
29. Emig, R., Zgierski-Johnston, C.M., Timmermann, V., Taberner, A.J., Nash, M.P., Kohl, P., and Peyronnet, R. (2021). Passive myocardial mechanical properties: meaning, measurement, models. Biophys. Rev. *13*, 587–610. https://doi.org/10.1007/s12551-021-00838-1.
30. Allijn, I., Ribeiro, M., Poot, A., Passier, R., and Stamatialis, D. (2020). Membranes for Modelling Cardiac Tissue Stiffness In Vitro Based on Poly(trimethylene carbonate) and Poly(ethylene glycol) Polymers. Membranes (Basel) *10*, 274. https://doi.org/10.3390/membranes10100274.
31. Fleischer, S., Shapira, A., Feiner, R., and Dvir, T. (2017). Modular assembly of thick multifunctional cardiac patches. Proc. Natl. Acad. Sci. USA *114*, 1898–1903. https://doi.org/10.1073/pnas.1615728114.
32. Boroumand, S., Haeri, A., Nazeri, N., and Rabbani, S. (2021). Review Insights In Cardiac Tissue Engineering: Cells, Scaffolds, and

Pharmacological Agents. Iran. J. Pharm. Res. *20*, 467–496. https://doi.org/10.22037/IJPR.2021.114730.15012.

33. Nam, S., Seo, B.R., Najibi, A.J., McNamara, S.L., and Mooney, D.J. (2023). Active tissue adhesive activates mechanosensors and prevents muscle atrophy. Nat. Mater. *22*, 249–259. https://doi.org/10.1038/s41563-022-01396-x.
34. Brady, B., King, G., Murphy, R.T., and Walsh, D. (2023). Myocardial strain: a clinical review. Ir. J. Med. Sci. *192*, 1649–1656. https://doi.org/10.1007/s11845-022-03210-8.
35. Sarmadi, M., Ta, C., VanLonkhuyzen, A.M., De Fiesta, D.C., Kanelli, M., Sadeghi, I., Behrens, A.M., Ingalls, B., Menon, N., Daristotle, J.L., et al. (2022). Experimental and computational understanding of pulsatile release mechanism from biodegradable core-shell microparticles. Sci. Adv. *8*, eabn5315. https://doi.org/10.1126/sciadv.abn5315.
36. Ifkovits, J.L., and Burdick, J.A. (2007). Review: photopolymerizable and degradable biomaterials for tissue engineering applications. Tissue Eng. *13*, 2369–2385. https://doi.org/10.1089/ten.2007.0093.
37. Bai, R., Yang, J., and Suo, Z. (2019). Fatigue of hydrogels. Eur. J. Mech. A Solids *74*, 337–370. https://doi.org/10.1016/j.euromechsol.2018.12.001.
38. Browning, M.B., Cereceres, S.N., Luong, P.T., and Cosgriff-Hernandez, E. M. (2014). Determination of the in vivo degradation mechanism of PEGDA hydrogels. J. Biomed. Mater. Res. A *102*, 4244–4251. https://doi.org/10.1002/jbm.a.35096.
39. Lappe, S., Mulac, D., and Langer, K. (2017). Polymeric nanoparticles - Influence of the glass transition temperature on drug release. Int. J. Pharm. *517*, 338–347. https://doi.org/10.1016/j.ijpharm.2016.12.025.
40. Marwah, H., Khare, S., Rawat, P., Singh, S., Kesharwani, P., Alam, M.S., Hamid, H., and Arora, S. (2022). Chapter 14. Strengths, limitations, and regulatory aspects of hybrid drug delivery systems. In Hybrid Nanomaterials for Drug Delivery, P. Kesharwani and N.K. Jain, eds. (Woodhead Publishing), pp. 339–355. https://doi.org/10.1016/B978-0-323-85754-3.00011-3.
41. Cao, Y., Gong, Y., Liu, L., Zhou, Y., Fang, X., Zhang, C., Li, Y., and Li, J. (2017). The use of human umbilical vein endothelial cells (HUVECs) as an in vitro model to assess the toxicity of nanoparticles to endothelium: a review. J. Appl. Toxicol. *37*, 1359–1369. https://doi.org/10.1002/jat.3470.
42. Andersen, F.A. (2005). Amended final report on the safety assessment of polyacrylamide and acrylamide residues in cosmetics. Int. J. Toxicol. *24*, 21–50. https://doi.org/10.1080/10915810590953842.
43. Wu, D.T., Freedman, B.R., Vining, K.H., Cuylear, D.L., Guastaldi, F.P.S., Levin, Y., and Mooney, D.J. (2023). Tough Adhesive Hydrogel for Intraoral Adhesion and Drug Delivery. J. Dent. Res. *102*, 497–504. https://doi.org/10.1177/00220345221148684.
44. Parlato, M., Reichert, S., Barney, N., and Murphy, W.L. (2014). Poly (ethylene glycol) hydrogels with adaptable mechanical and degradation properties for use in biomedical applications. Macromol. Biosci. *14*, 687–698. https://doi.org/10.1002/mabi.201300418.
45. Simón-Yarza, T., Formiga, F.R., Tamayo, E., Pelacho, B., Prosper, F., and Blanco-Prieto, M.J. (2012). Vascular endothelial growth factor-delivery systems for cardiac repair: an overview. Theranostics *2*, 541–552. https://doi.org/10.7150/thno.3682.
46. Santoro, F., and Sahara, M. (2015). A specified therapeutic window for neuregulin-1 to regenerate neonatal heart muscle. Ann. Transl. Med. *3*, 249. https://doi.org/10.3978/j.issn.2305-5839.2015.09.38.
47. Parichatikanond, W., Luangmonkong, T., Mangmool, S., and Kurose, H. (2020). Therapeutic Targets for the Treatment of Cardiac Fibrosis and Cancer: Focusing on TGF-β Signaling. Front. Cardiovasc. Med. *7*, 34. https://doi.org/10.3389/fcvm.2020.00034.
48. Wang, Y., Wei, J., Zhang, P., Zhang, X., Wang, Y., Chen, W., Zhao, Y., and Cui, X. (2022). Neuregulin-1, a potential therapeutic target for cardiac repair. Front. Pharmacol. *13*, 945206. https://doi.org/10.3389/fphar.2022.945206.
49. Ikeuchi, M., Tsutsui, H., Shiomi, T., Matsusaka, H., Matsushima, S., Wen, J., Kubota, T., and Takeshita, A. (2004). Inhibition of TGF-beta signaling exacerbates early cardiac dysfunction but prevents late remodeling after infarction. Cardiovasc. Res. *64*, 526–535. https://doi.org/10.1016/j.cardiores.2004.07.017.
50. Zhao, Y., Wang, E.Y., Lai, F.B.L., Cheung, K., and Radisic, M. (2023). Organs-on-a-chip: a union of tissue engineering and microfabrication. Trends Biotechnol. *41*, 410–424. https://doi.org/10.1016/j.tibtech.2022.12.018.
51. Litviňuková, M., Talavera-López, C., Maatz, H., Reichart, D., Worth, C.L., Lindberg, E.L., Kanda, M., Polanski, K., Heinig, M., Lee, M., et al. (2020). Cells of the adult human heart. Nature *588*, 466–472. https://doi.org/10.1038/s41586-020-2797-4.
52. Tucker, N.R., Chaffin, M., Fleming, S.J., Hall, A.W., Parsons, V.A., Bedi, K. C., Jr., Akkad, A.D., Herndon, C.N., Arduini, A., Papangeli, I., et al. (2020). Transcriptional and Cellular Diversity of the Human Heart. Circulation *142*, 466–482. https://doi.org/10.1161/CIRCULATIONAHA.119.045401.
53. Melincovici, C.S., Boşca, A.B., Şuşman, S., Mărginean, M., Mihu, C., Istrate, M., Moldovan, I.M., Roman, A.L., and Mihu, C.M. (2018). Vascular endothelial growth factor (VEGF) - key factor in normal and pathological angiogenesis. Rom. J. Morphol. Embryol. *59*, 455–467.
54. Cho, H., Macklin, B.L., Lin, Y.Y., Zhou, L., Lai, M.J., Lee, G., Gerecht, S., and Duh, E.J. (2020). iPSC-derived endothelial cell response to hypoxia via SDF1a/CXCR4 axis facilitates incorporation to revascularize ischemic retina. JCI Insight *5*, e131828. https://doi.org/10.1172/jci.insight.131828.
55. Potente, M., Gerhardt, H., and Carmeliet, P. (2011). Basic and therapeutic aspects of angiogenesis. Cell *146*, 873–887. https://doi.org/10.1016/j.cell.2011.08.039.
56. Kong, P., Christia, P., and Frangogiannis, N.G. (2014). The pathogenesis of cardiac fibrosis. Cell. Mol. Life Sci. *71*, 549–574. https://doi.org/10.1007/s00018-013-1349-6.
57. Zhao, Y., Xiong, W., Li, C., Zhao, R., Lu, H., Song, S., Zhou, Y., Hu, Y., Shi, B., and Ge, J. (2023). Hypoxia-induced signaling in the cardiovascular system: pathogenesis and therapeutic targets. Signal Transduct. Target. Ther. *8*, 431. https://doi.org/10.1038/s41392-023-01652-9.
58. Ma, W., Wei, S., Zhang, B., and Li, W. (2020). Molecular Mechanisms of Cardiomyocyte Death in Drug-Induced Cardiotoxicity. Front. Cell Dev. Biol. *8*, 434. https://doi.org/10.3389/fcell.2020.00434.
59. Sun, K., Li, Y.-Y., and Jin, J. (2021). A double-edged sword of immunomicroenvironment in cardiac homeostasis and injury repair. Signal Transduct. Target. Ther. *6*, 79. https://doi.org/10.1038/s41392-020-00455-6.
60. Awada, H.K., Johnson, N.R., and Wang, Y. (2015). Sequential delivery of angiogenic growth factors improves revascularization and heart function after myocardial infarction. J. Control. Release *207*, 7–17. https://doi.org/10.1016/j.jconrel.2015.03.034.
61. RayChaudhury, A., Elkins, M., Kozien, D., and Nakada, M.T. (2001). Regulation of PECAM-1 in endothelial cells during cell growth and migration. Exp. Biol. Med. (Maywood) *226*, 686–691. https://doi.org/10.1177/153537020222600715.
62. Samsamshariat, S.A., Samsamshariat, Z.A., and Movahed, M.R. (2005). A novel method for safe and accurate left anterior descending coronary artery ligation for research in rats. Cardiovasc. Revasc. Med. *6*, 121–123. https://doi.org/10.1016/j.carrev.2005.07.001.
63. Blenck, C.L., Harvey, P.A., Reckelhoff, J.F., and Leinwand, L.A. (2016). The Importance of Biological Sex and Estrogen in Rodent Models of Cardiovascular Health and Disease. Circ. Res. *118*, 1294–1312. https://doi.org/10.1161/CIRCRESAHA.116.307509.
64. Radisic, M., and Christman, K.L. (2013). Materials science and tissue engineering: repairing the heart. Mayo Clin. Proc. *88*, 884–898. https://doi.org/10.1016/j.mayocp.2013.05.003.
65. Walker, B.W., Lara, R.P., Yu, C.H., Sani, E.S., Kimball, W., Joyce, S., and Annabi, N. (2019). Engineering a naturally-derived adhesive and

conductive cardiopatch. Biomaterials *207*, 89–101. https://doi.org/10.1016/j.biomaterials.2019.03.015.

66. Lopez-Jimenez, F., Wu, C.O., Tian, X., O'Connor, C., Rich, M.W., Burg, M. M., Sheps, D., Raczynski, J., Somers, V.K., and Jaffe, A.S. (2008). Weight change after myocardial infarction–the Enhancing Recovery in Coronary Heart Disease patients (ENRICHD) experience. Am. Heart J. *155*, 478–484. https://doi.org/10.1016/j.ahj.2007.10.026.
67. Jacob, R., and Khan, M. (2018). Cardiac Biomarkers: What Is and What Can Be. Indian J. CardioVasc Dis Women WINCARS *3*, 240–244. https://doi.org/10.1055/s-0039-1679104.
68. Rupert, C.E., and Coulombe, K.L. (2015). The roles of neuregulin-1 in cardiac development, homeostasis, and disease. Biomark. Insights *10*, 1–9. https://doi.org/10.4137/BMI.S20061.
69. Gao, H., Liu, S., Qin, S., Yang, J., Yue, T., Ye, B., Tang, Y., Feng, J., Hou, J., and Danzeng, D. (2024). Injectable hydrogel-based combination therapy for myocardial infarction: a systematic review and Meta-analysis of preclinical trials. BMC Cardiovasc. Disord. *24*, 119. https://doi.org/10.1186/s12872-024-03742-0.
70. Cao, Y., Fan, R., Zhu, K., and Gao, Y. (2024). Advances in Functionalized Hydrogels in the Treatment of Myocardial Infarction and Drug-Delivery Strategies. ACS Appl. Mater. Interfaces *16*, 48880–48894. https://doi.org/10.1021/acsami.4c09623.
71. Wu, Y., Chang, T., Chen, W., Wang, X., Li, J., Chen, Y., Yu, Y., Shen, Z., Yu, Q., and Zhang, Y. (2021). Release of VEGF and BMP9 from injectable alginate based composite hydrogel for treatment of myocardial infarction. Bioact. Mater. *6*, 520–528. https://doi.org/10.1016/j.bioactmat.2020.08.031.
72. Daly, A.C., Riley, L., Segura, T., and Burdick, J.A. (2020). Hydrogel microparticles for biomedical applications. Nat. Rev. Mater. *5*, 20–43. https://doi.org/10.1038/s41578-019-0148-6.
73. Wang, E.Y., Sarmadi, M., Ying, B., Jaklenec, A., and Langer, R. (2023). Recent advances in nano- and micro-scale carrier systems for controlled delivery of vaccines. Biomaterials *303*, 122345. https://doi.org/10.1016/j.biomaterials.2023.122345.
74. Tang, J., Wang, J., Huang, K., Ye, Y., Su, T., Qiao, L., Hensley, M.T., Caranasos, T.G., Zhang, J., Gu, Z., et al. (2018). Cardiac cell-integrated microneedle patch for treating myocardial infarction. Sci. Adv. *4*, eaat9365. https://doi.org/10.1126/sciadv.aat9365.
75. Montgomery, M., Ahadian, S., Davenport Huyer, L., Lo Rito, M., Civitarese, R.A., Vanderlaan, R.D., Wu, J., Reis, L.A., Momen, A., Akbari, S., et al. (2017). Flexible shape-memory scaffold for minimally invasive delivery of functional tissues. Nat. Mater. *16*, 1038–1046. https://doi.org/10.1038/nmat4956.
76. Wendel, J.S., Ye, L., Tao, R., Zhang, J., Zhang, J., Kamp, T.J., and Tranquillo, R.T. (2015). Functional Effects of a Tissue-Engineered Cardiac Patch From Human Induced Pluripotent Stem Cell-Derived Cardiomyocytes in a Rat Infarct Model. Stem Cells Transl. Med. *4*, 1324–1332. https://doi.org/10.5966/sctm.2015-0044.
77. Wang, Z., Long, D.W., Huang, Y., Chen, W.C.W., Kim, K., and Wang, Y. (2019). Decellularized neonatal cardiac extracellular matrix prevents widespread ventricular remodeling in adult mammals after myocardial infarction. Acta Biomater. *87*, 140–151. https://doi.org/10.1016/j.actbio.2019.01.062.
78. Liao, J., Li, X., and Fan, Y. (2023). Prevention strategies of postoperative adhesion in soft tissues by applying biomaterials: Based on the mechanisms of occurrence and development of adhesions. Bioact. Mater. *26*, 387–412. https://doi.org/10.1016/j.bioactmat.2023.02.026.
79. Fatehi Hassanabad, A., Zarzycki, A.N., Jeon, K., Dundas, J.A., Vasanthan, V., Deniset, J.F., and Fedak, P.W.M. (2021). Prevention of Post-Operative Adhesions: A Comprehensive Review of Present and Emerging Strategies. Biomolecules *11*, 1027. https://doi.org/10.3390/biom11071027.
80. Capella-Monsonís, H., Kearns, S., Kelly, J., and Zeugolis, D.I. (2019). Battling adhesions: from understanding to prevention. BMC Biomed. Eng. *1*, 5. https://doi.org/10.1186/s42490-019-0005-0.
81. Cannata, A., Petrella, D., Russo, C.F., Bruschi, G., Fratto, P., Gambacorta, M., and Martinelli, L. (2013). Postsurgical intrapericardial adhesions: mechanisms of formation and prevention. Ann. Thorac. Surg. *95*, 1818–1826. https://doi.org/10.1016/j.athoracsur.2012.11.020.
82. Fang, Y., McGrail, D.J., Sun, C., Labrie, M., Chen, X., Zhang, D., Ju, Z., Vellano, C.P., Lu, Y., Li, Y., et al. (2019). Sequential Therapy with PARP and WEE1 Inhibitors Minimizes Toxicity while Maintaining Efficacy. Cancer Cell *35*, 851–867.e7. https://doi.org/10.1016/j.ccell.2019.05.001.
83. Eshaghi, B., Alsharif, N., An, X., Akiyama, H., Brown, K.A., Gummuluru, S., and Reinhard, B.M. (2020). Stiffness of HIV-1 Mimicking Polymer Nanoparticles Modulates Ganglioside-Mediated Cellular Uptake and Trafficking. Adv. Sci. (Weinh) *7*, 2000649. https://doi.org/10.1002/advs.202000649.
84. Kuzmanov, U., Wang, E.Y., Vanderlaan, R., Kim, D.H., Lee, S.-H., Hadipour-Lakmehsari, S., Guo, H., Zhao, Y., McFadden, M., Sharma, P., et al. (2020). Mapping signalling perturbations in myocardial fibrosis via the integrative phosphoproteomic profiling of tissue from diverse sources. Nat. Biomed. Eng. *4*, 889–900. https://doi.org/10.1038/s41551-020-0585-y.

CELBIO, Volume *2*

Supplemental information

TIMED: Temporal intervention with microparticle encapsulation and delivery—A programmed release system for post-myocardial infarction therapy

Erika Yan Wang, Elizabeth A. Calle, Binbin Ying, Behnaz Eshaghi, Linzixuan Zhang, Xin Yang, Stacey Qiaohui Lin, Jooli Han, Alanna G. Backx, Yuting Huang, Sevinj Mursalova, Chuhan Joyce Qi, Yi Liu, Robert Langer, and Ana Jaklenec

Supplementary Material List

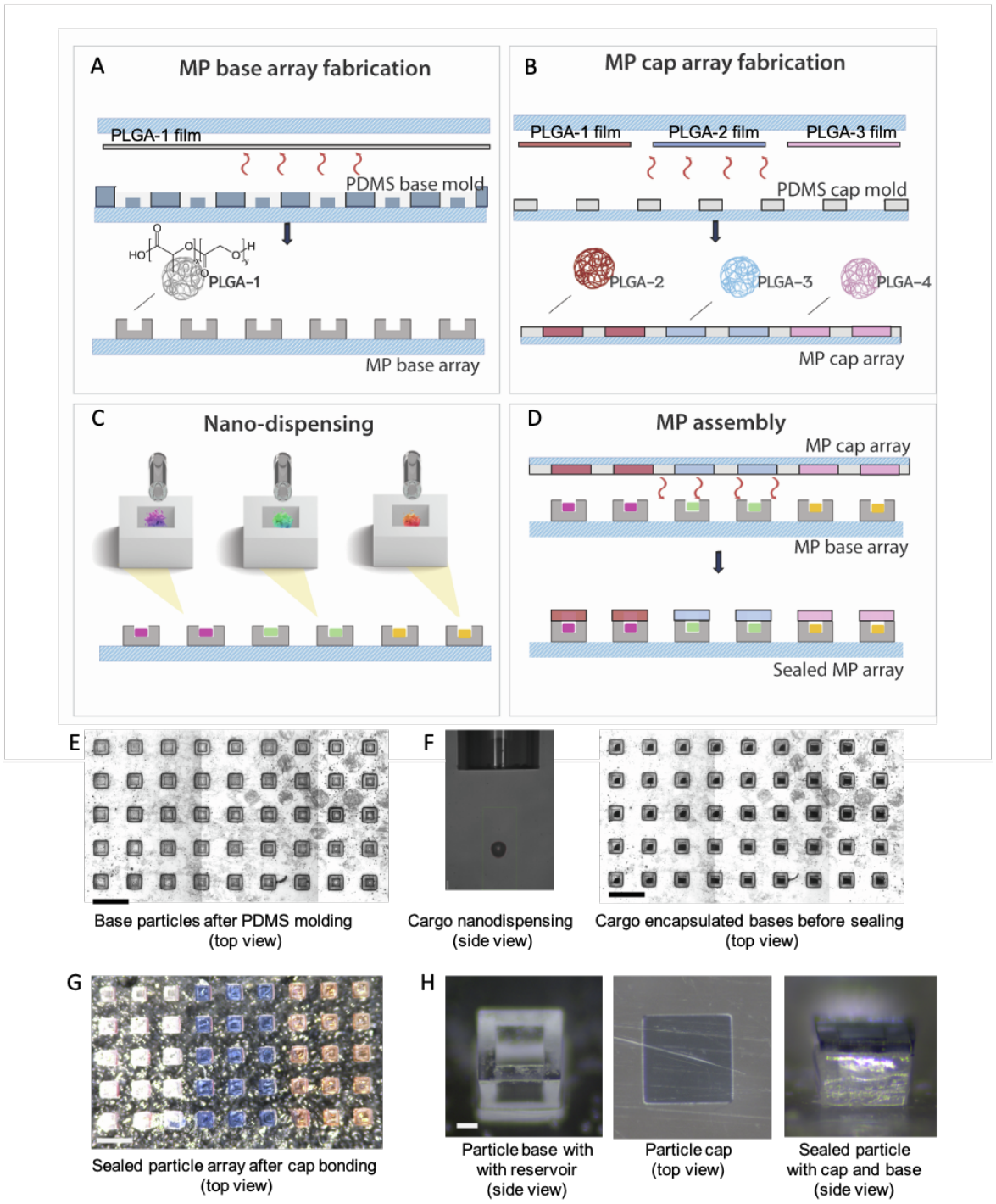

Fig. S1. Microfabrication process of the drug-load PLGA microparticle array with representative optical images of each step. *(**A**) Microfabrication of the microparticle base array. (**B**) Microfabrication of the microparticle cap array. (**C**) Nano-dispensing of drug molecules and excipients onto the base array. (**D**) Assembly of the microparticles using 3D stamping and thermo-bonding of the base and cap arrays.* ***(E–H)***

Representative optical images of fabrication steps. ***(E)*** *Base particle arrays formed by PLGA casting (scale bar = 1 mm).* ***(F)*** *Cargo loading process using a piezoelectric nano-dispenser; dark spots in the reservoirs indicate deposited drug/excipient cargos (scale bar=1 mm).* ***(G)*** *Sealed particle array after thermo-bonding of base and cap arrays (scale bar=1 mm).* ***(H)*** *Magnified top and side views of individual sealed particles (scale bar=100 μm).*

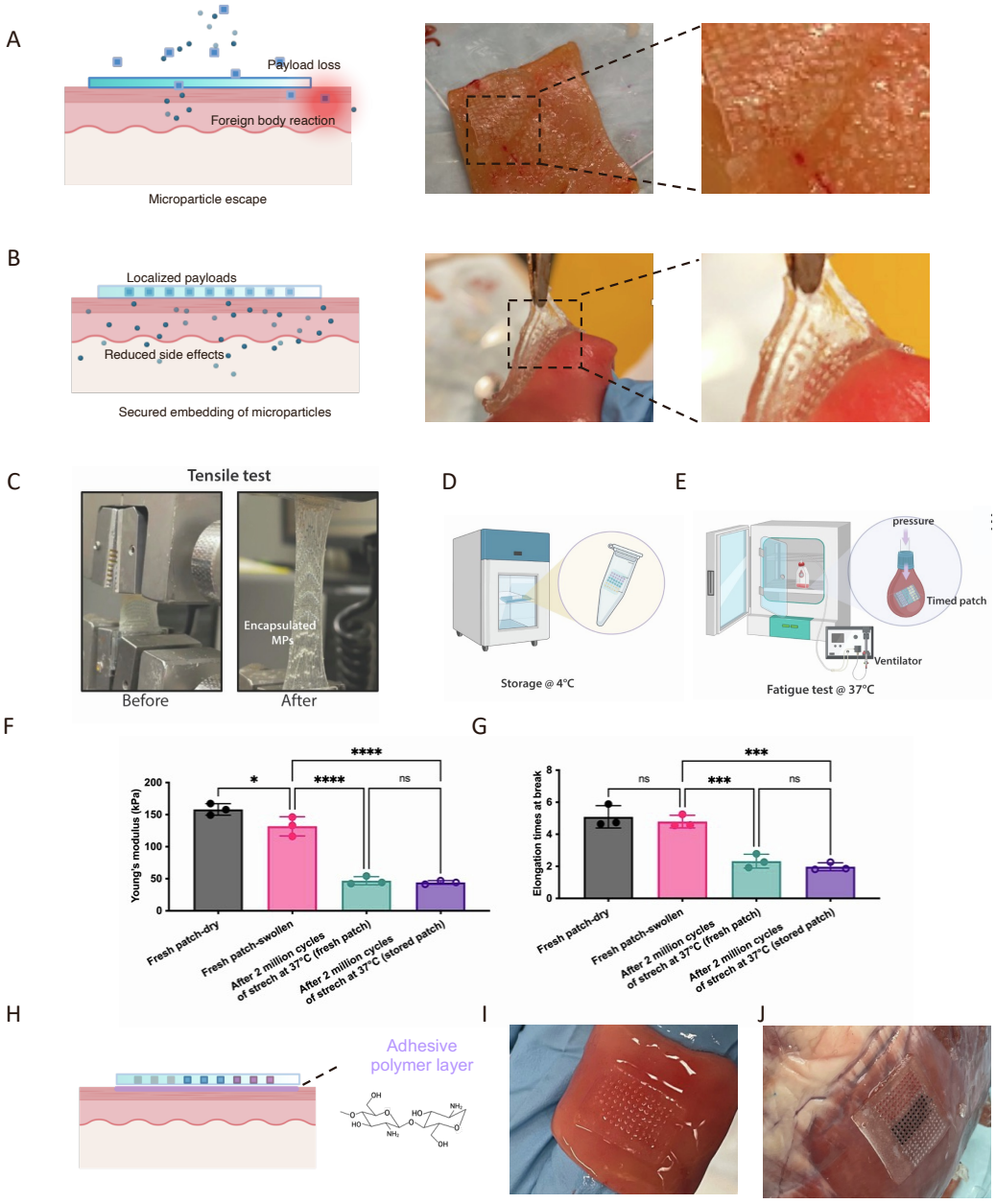

Fig. S2. Assessing TIMED patch suitability for implantation on surgical surfaces. *(**A** to **B**) Schematics illustrating micro-carrier detachment from a non-encapsulated system versus the fully encapsulated TIMED patch, along with corresponding images showing dislodged particles on tissue surface versus particles fully embedded in the TIMED patch matrix. (**C**) Representative images of a TIMED patch pre- and post-application of tensile stress, demonstrating patch integrity and secure encapsulation of microparticles. (**D** to **E**) Schematic illustrating tested conditions, including the storage conditions of the TIMED patch at 4°C and cyclic stretching tests at 37°C. (**F** to **G**) Mechanical performance of the patch under different conditions. Fresh (Fresh patch-dry = tested after fabrication without hydration; Fresh*

*patch-swollen = hydrated in saline for 1h to reach a swollen state before testing) and after fatigue testing (Fresh vs. Stored). (**F**) Young's modulus determined by tensile testing. (**G**) Elongation at break point measured by tensile testing. Data are shown as mean ± SD. n = 3. Statistical analysis was performed using one-way ANOVA followed by Tukey's multiple comparisons test. (**H**) Schematic illustrating the application of a chitosan adhesive layer to adhere the TIMED patch to tissue surface. (**I** to **J**) Images showing TIMED patch adhered to ex vivo pig intestinal (I) and cardiac (J) tissue surfaces, utilizing the chitosan adhesive for secure attachment.*

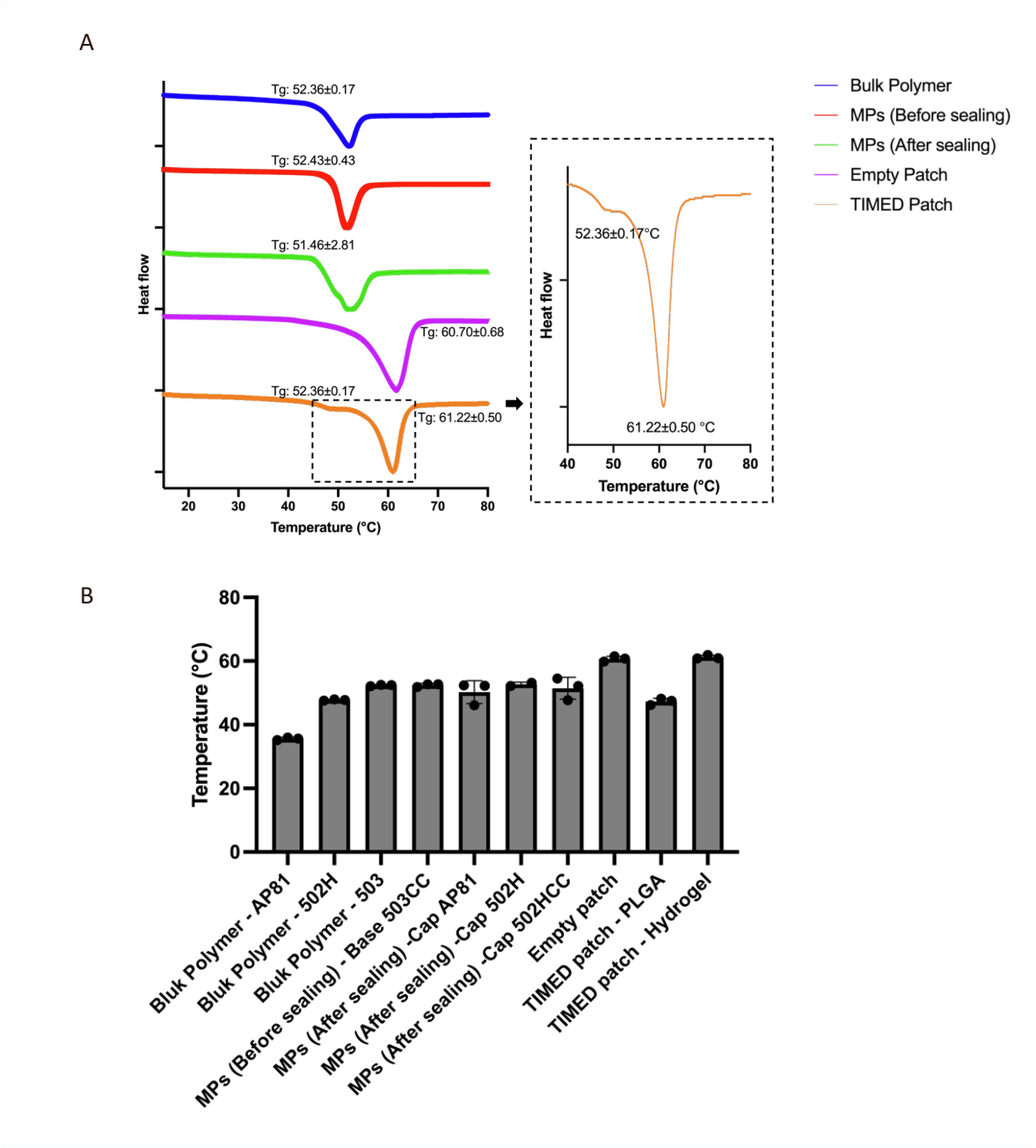

Fig. S3. Differential scanning calorimetry (DSC) assessment of the TIMED system. *(**A**) Representative DSC thermograms of bulk polymer, microparticles (MPs) both before and after sealing, empty patches, and TIMED patches. The peak values are reported on the plots as glass transition temperature (Tg). Curves are vertically shifted for visual clarity. The curve of the TIMED patch is shown in the zoomed-in box for clear visualization of the double peaks. (**B**) Peak values of DSC thermograms of PLGA bulk polymer, microparticles (MPs) both before and after sealing, empty patches, and TIMED patches. All DSC experiments were performed in triplicates.*

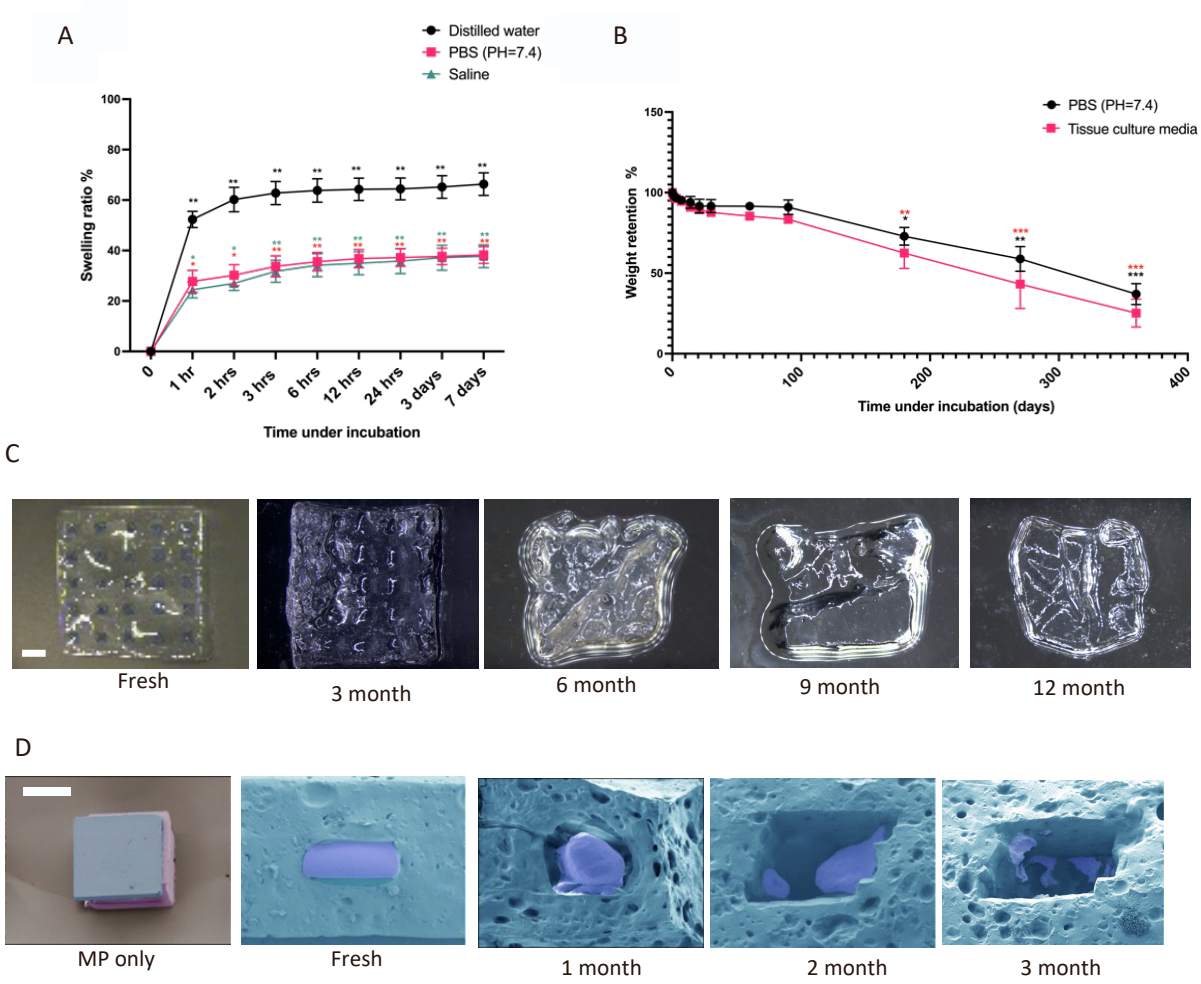

Fig. S4. Swelling and degradation properties of the TIMED patch. *(**A**) Evaluation of the swelling dynamics of the TIMED patch in immersion media including distilled water, Phosphate Buffered Saline (PBS), and saline solution, to simulate physiological conditions. Data analyzed by one-way repeated measures ANOVA vs baseline (0 hr) within each group. n=5. (**B**) Profiling the degradation kinetics of the TIMED patch in PBS and culture media at 37°C, reflecting the in vivo thermal environment. Data analyzed by one-way repeated measures ANOVA vs baseline (day 0) within each group. n=3. (**C**) Comparative imaging of the TIMED patch at initial incubation and after up to one year, showing degraded microparticles within the patch matrix. Scale bar= 1 mm. (**D**) Scanning Electron Microscopy (SEM) images showing microparticles before encapsulation, after freshly encapsulated in the hydrogel matrix, and after 1- 3 months of incubation, illustrating the MP degradation process in the matrix. The microparticle base is pseudo-colored in purple, microparticle cap is pseudo-colored in blue, for differentiation from the hydrogel. Scale bar=300μm.*

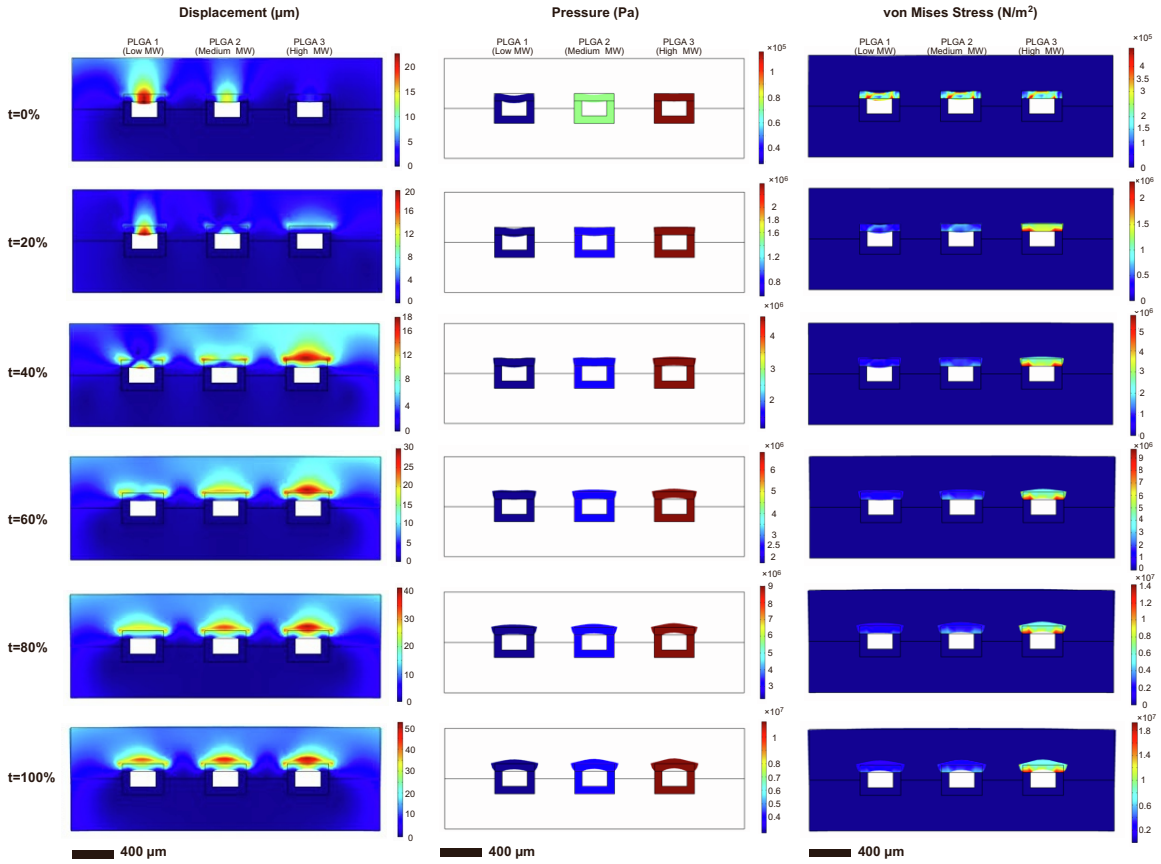

Fig. S5. Predictive simulation of release kinetics within a singular device. *Computational simulation of a TIMED patch containing patterned PLGA particles with differing molecular weights, illustrating the potential for tailored release profiles. The three cubic particles represent distinct PLGA formulations that vary in molecular weight. The deformation of the cap started from the center, and then progressed toward the edge and exterior parts of the cap for all the formulations. Scale bars =400 μm.*

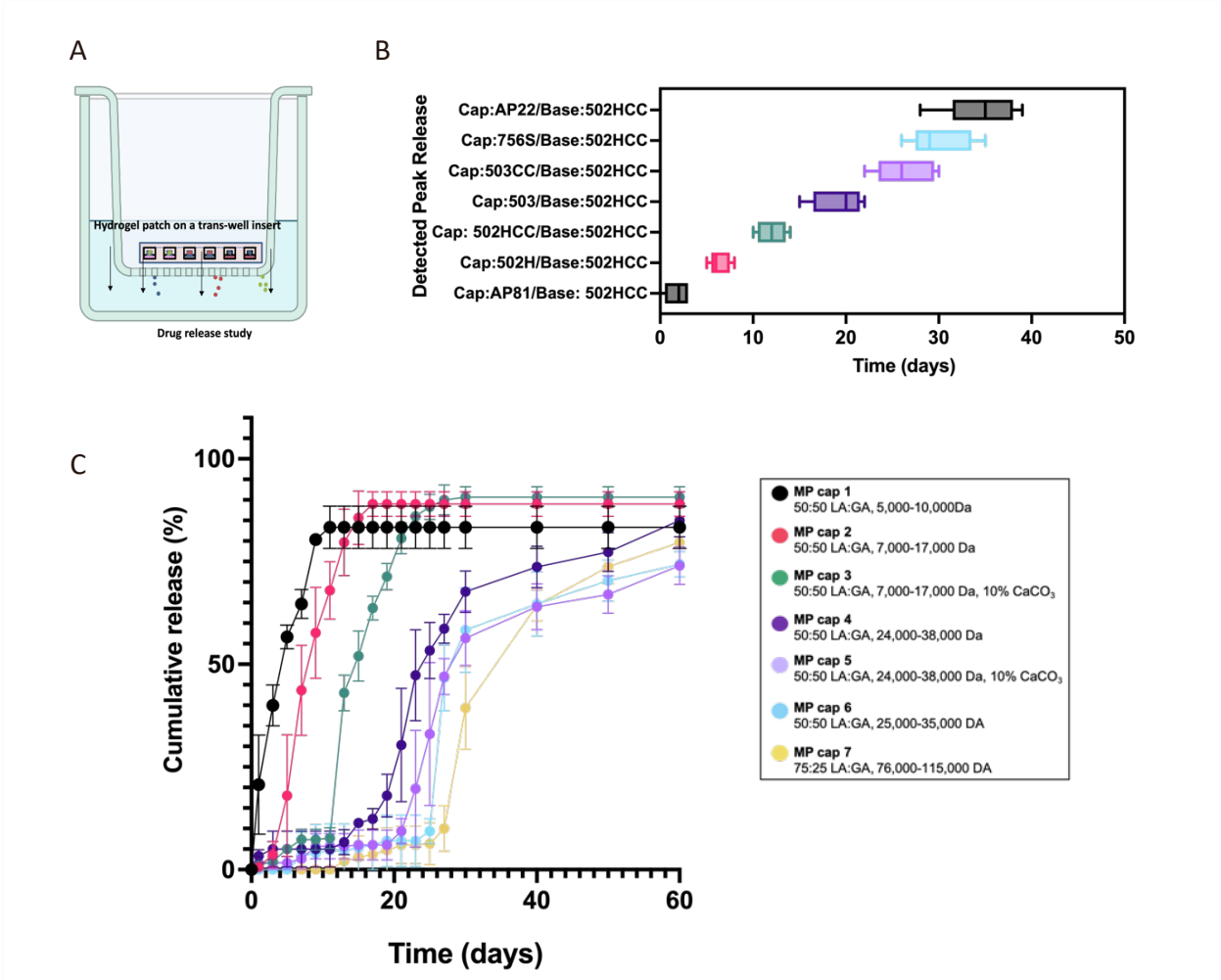

Fig. S6. in vitro screening of drug release kinetics from the TIMED system using 502HCC PLGA bases. *(**A**) Schematic representation of the in vitro screening setup utilizing a trans-well model to empirically validate release kinetics. (**B**) Initial time of peak release from each MP composition with 502HCC bases. (**C**) Release kinetics of dextran dye as model molecules from MPs fabricated with a panel of different cap materials on 502HCC bases. n=3.*

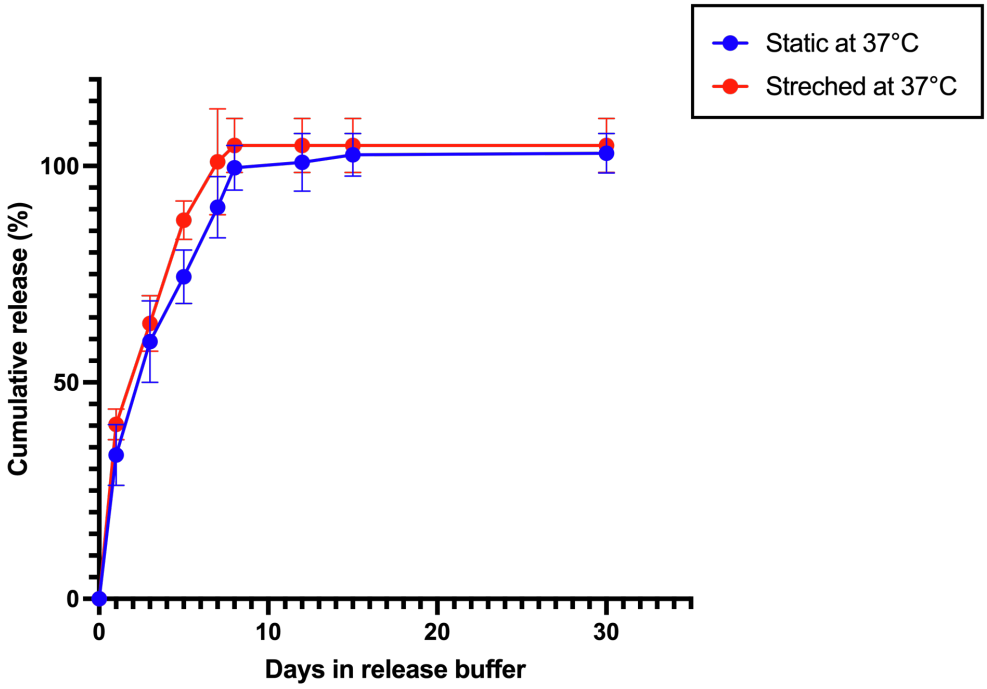

Fig. S7. ***Effect of cyclic stretch on drug release kinetics.*** *Cumulative release kinetics of AP81 (one-day release) microparticles embedded in fresh, swollen patches subjected to 300 beats per minute cyclic stretch (53.5% strain) at 37°C, compared to a static control. $n \geq 3$.*

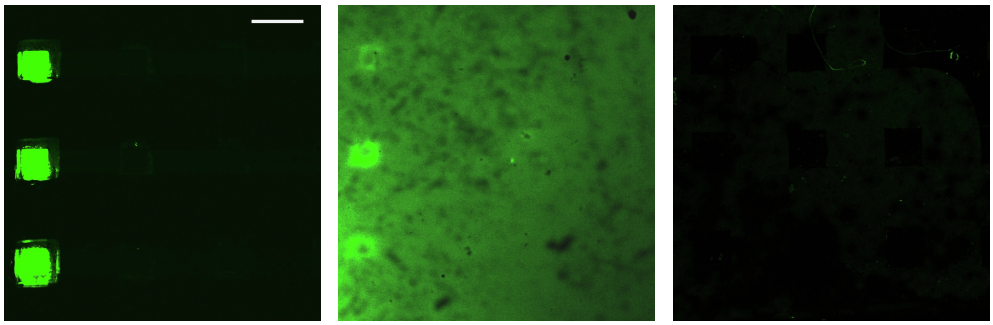

Fig. S8. Diffusion of dye molecules across the patch. *10 kDa Alexa Fluor™ 488-labeled dextran model dye was loaded into a single array of AP81 (one-day release) microparticles, and patch diffusion was monitored over the course of release. Images captured before incubation, at peak release, and post-release demonstrate uniform distribution of the dye within the hydrogel matrix. Scale bar=500 µm.*

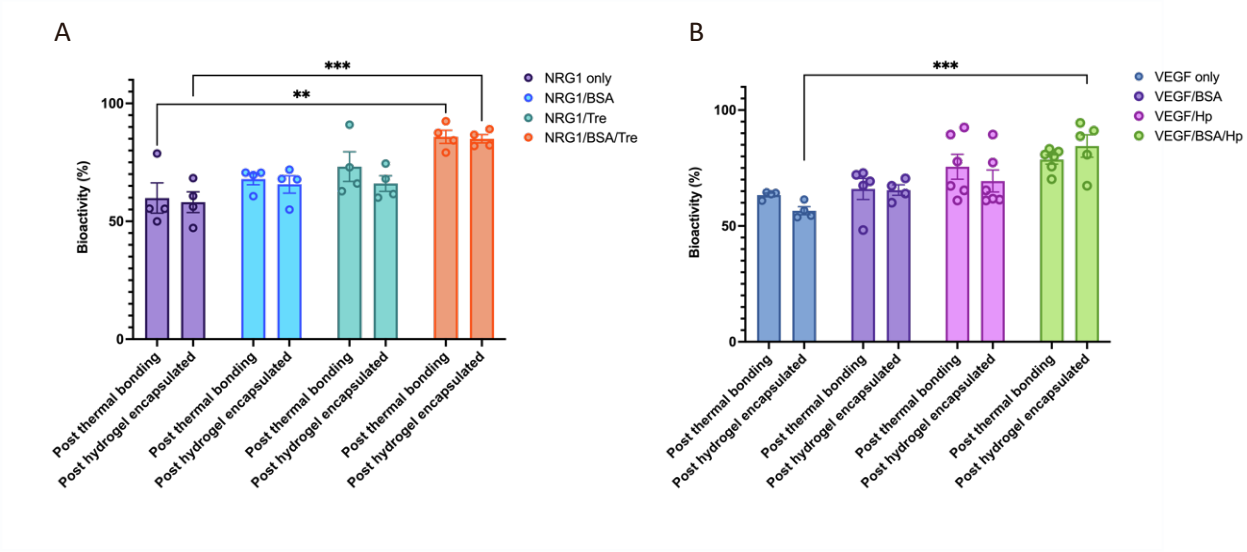

Fig. S9. Screening of stabilizing excipients for protein bioactivity preservation. *VEGF (A) and NRG1 (B) were co-loaded with excipients, and their bioactivity was assessed using functional assays. NRG1 bioactivity was evaluated via MCF-7 proliferation assay, where MCF-7, a human breast cancer cell line, proliferates in response to NRG1 stimulation, quantified by MTT assay. VEGF bioactivity was tested using the Promega VEGF Bioassay, a reporter-based system that measures VEGF receptor activation via luciferase expression. Bioactivity was assessed post-particle sealing and post-hydrogel fabrication to determine the formulation that best preserves protein function. $n \geq 4$.*

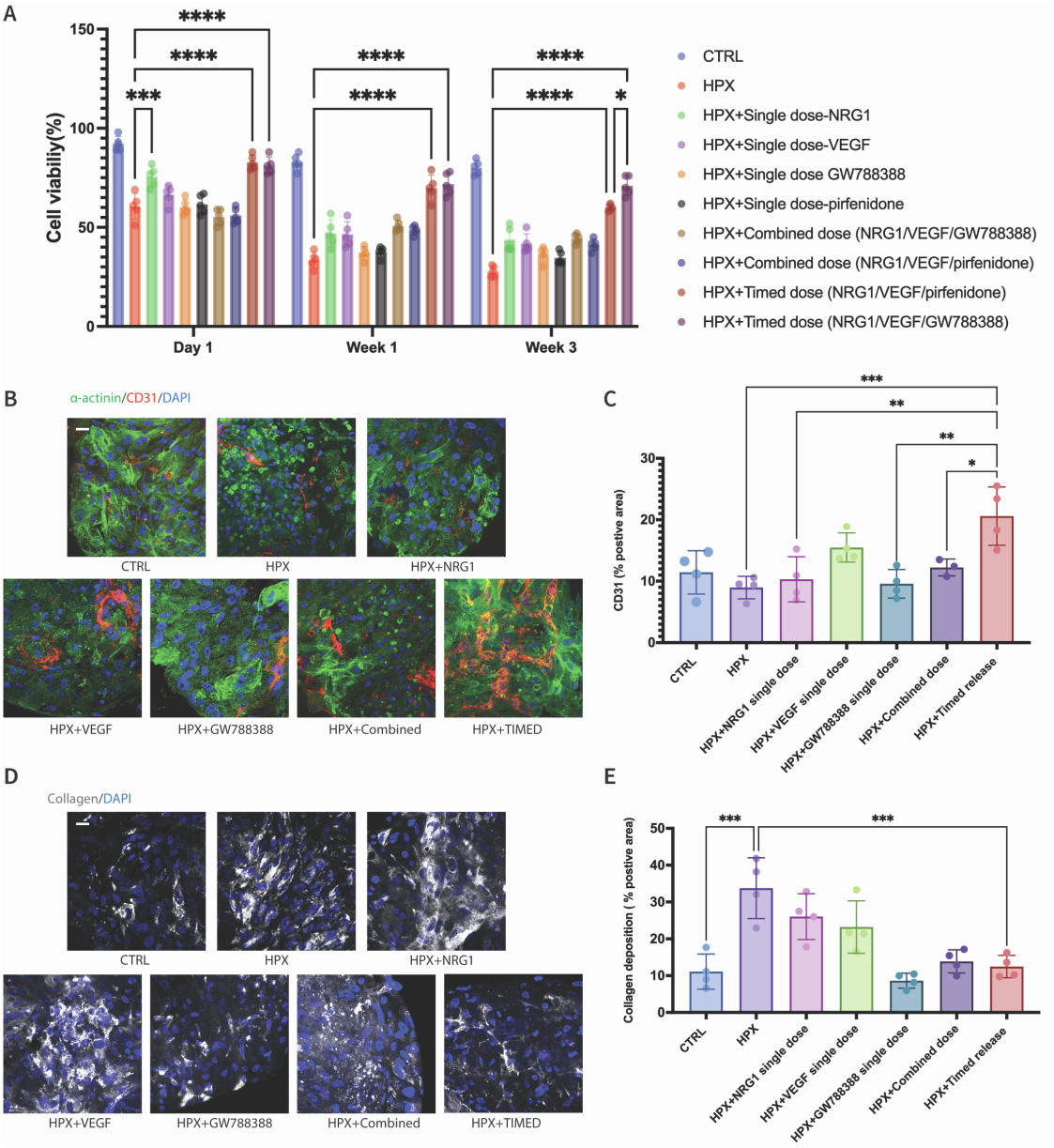

Fig. S10. Validation of TIMED release efficacy over single-dose administration. *(A) Cell viability screening using across different treatment combinations over the course of three weeks (n ≥ 3). (B) Representative images of cardiac spheres stained for α-actinin (cardiomyocytes) and CD31 (endothelial cells) to assess cellular composition and angiogenesis at different time points. Scale bar = 10μm.(C) Quantification of CD31 coverage, indicating neovascularization within cardiac spheres at multiple time points (n ≥ 3). (D) Representative images of cardiac spheres stained for collagen, evaluating fibrotic deposition over three weeks. Scale bar = 10 μm. (E) Quantitative analysis of collagen coverage, serving as a fibrosis metric within each tissue sample across the cultivation period. n ≥ 3.*

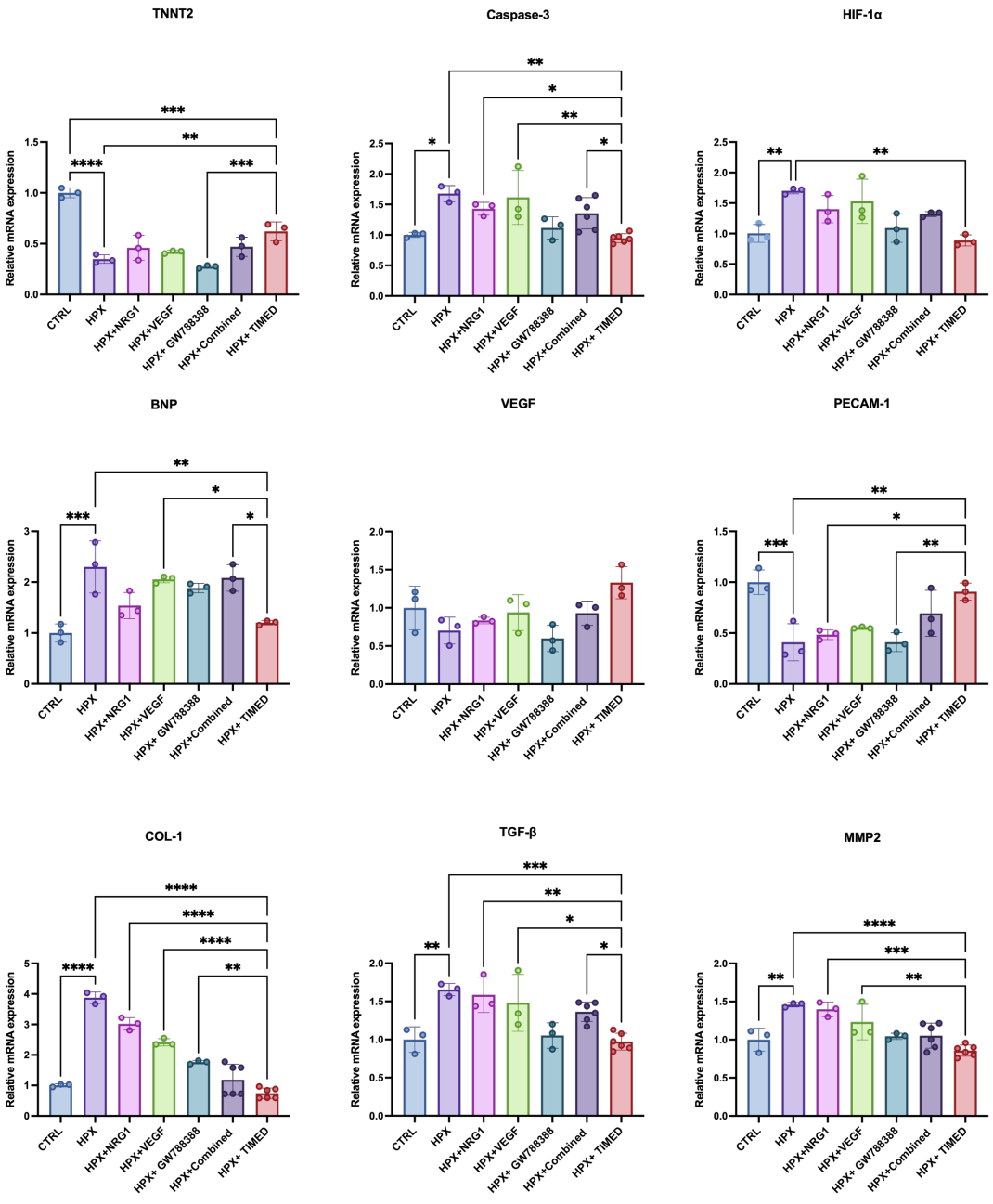

Fig. S11. RT-PCR analysis validating the gene expression of key regulatory pathways at the three-week endpoint across different treatment groups. *Gene expression was quantified using the ΔΔCT method and normalized to the control group. Combined single dose = all agents at t0 (post-hypoxia); TIMED = TIMED patch placed on the insert above the wells, releasing agents sequentially to mirror programmed delivery. $n \geq 3$.*

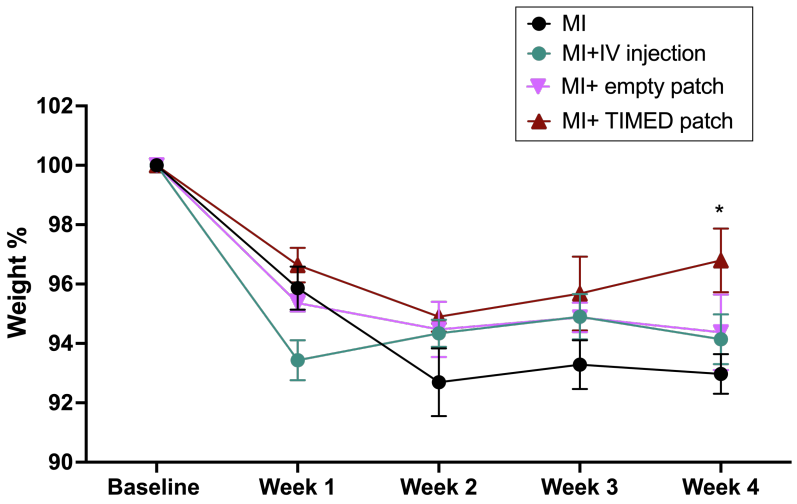

Fig. S12. Weight change over the course of in vivo study across different groups. *All post-surgery weights were normalized to each animal's baseline pre-surgery weight. Statistical analysis was performed using two-way repeated measures ANOVA with Tukey's post hoc test. n≥5.*

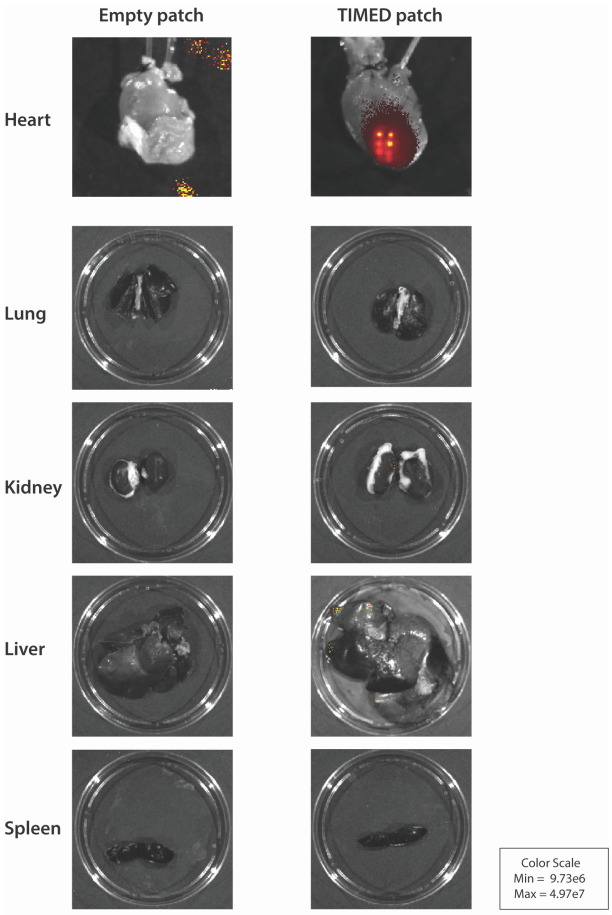

Fig. S13. IVES imaging of systemic drug distribution following TIMED patch implantation. *The TIMED patch was loaded with Dextran (10K) Flamma® 774, a far-red fluorescent dye selected to minimize tissue autofluorescence. Ex vivo IVES imaging was performed post-release to assess drug distribution. Fluorescence signals were detected in the heart, confirming localized release, while no detectable signal was observed in secondary organs, including the lungs, liver, spleen, and kidneys, indicating minimal systemic exposure and off-target effects.*

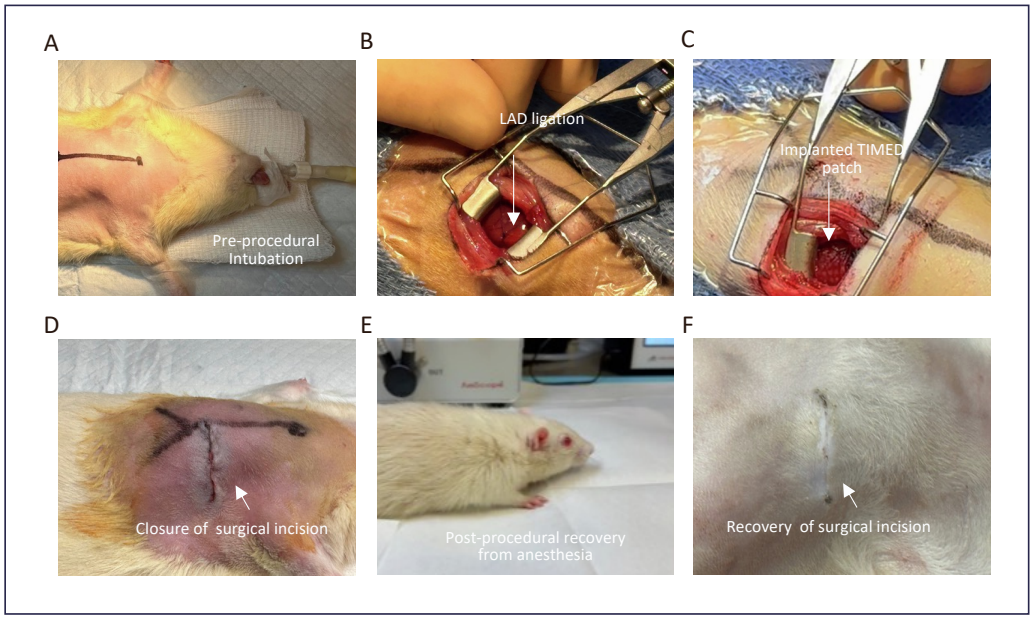

Fig. S14. Surgical procedure of TIMED patch implantation. *(**A**) Image illustrating intratracheal intubation prior to incision. (**B**) Surgical procedure for left anterior descending (LAD) ligation, depicted with 6-0 Prolene suture, with blanching of the affected myocardium below the ligation point. (**C**) Image displaying the TIMED patch implanted on the heart. The patch is sutured onto the heart following LAD ligation, adhering to the surface of a beating heart, with visible microparticles. (**D**) Image depicting completed chest and skin closure post LAD ligation and TIMED patch implantation. (**E**) Image illustrating the animal's recovery from anesthesia after surgery. (**F**) Image demonstrating the incision's recovery after surgery, reflecting optimal surgical practice and animal's overall wellbeing.*

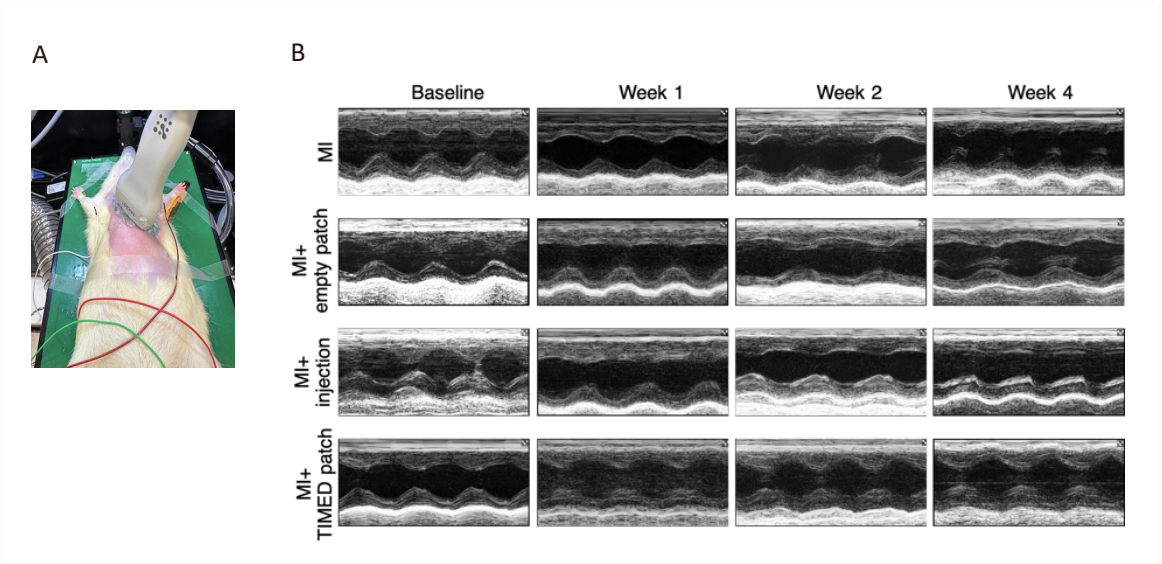

Fig. S15. Ultrasound setup and assessment for in vivo study. *(**A**) Demonstration of ultrasound imaging process post-surgery. The rat was imaged under anesthesia, with echocardiography conducted using a MX201 transducer probe. (**B**) Representative M-mode echocardiography images through the course of experiment, as a visual indicator of cardiac motion.*

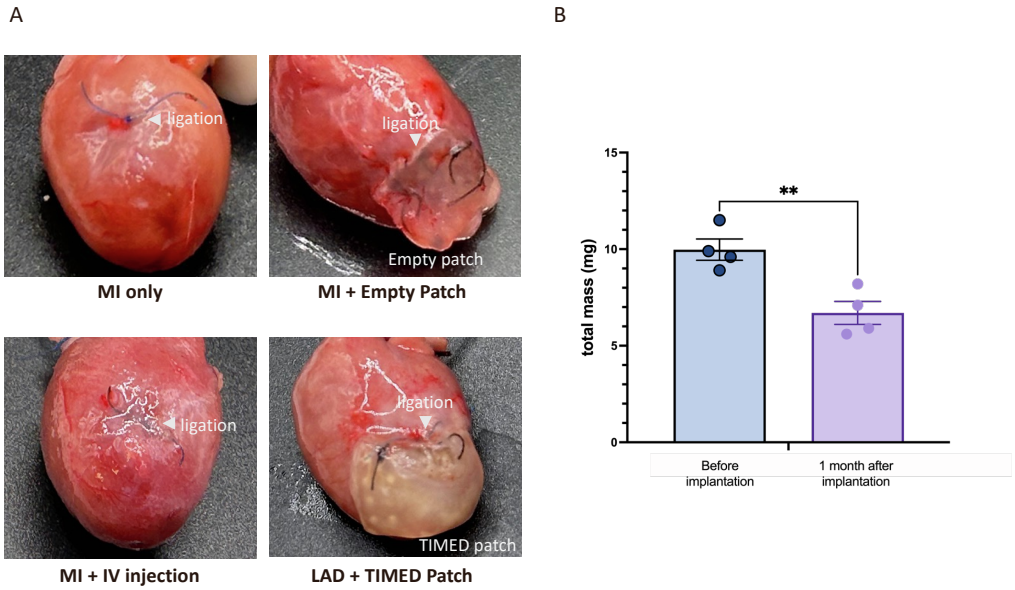

Fig. S16. Representative images of rat hearts obtained at endpoint and degradation assessment. *(A) Hearts post-extraction from the chest cavity and subsequent perfusion with potassium. Ligation points and patch positions are labeled. (**B**) Quantification dry mass of the TIMED patch before implantation and at the 1-month endpoint. Patch mass was determined after lyophilization to ensure accurate quantification of retained polymer content. Statistical analysis was performed using an unpaired two-tailed Student's t-test. n=4.*

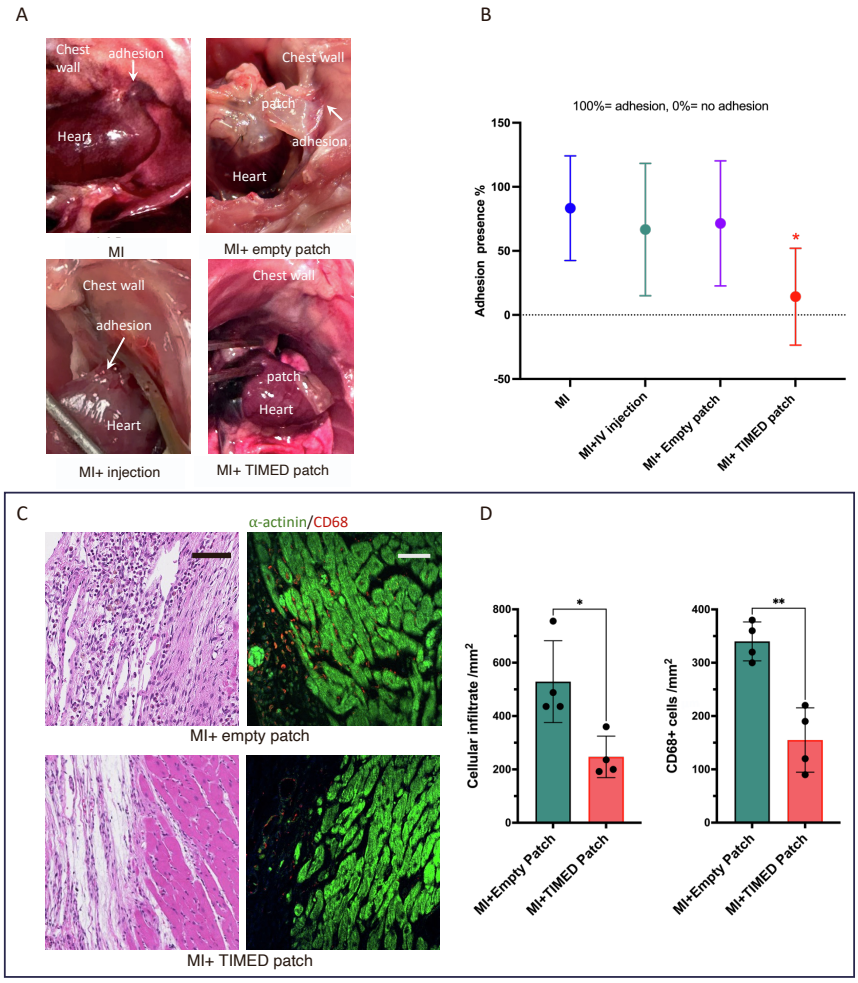

Fig. S17. Evaluation of postoperative surgical adhesion across experimental cohorts at 4-week endpoint. *(**A**) Representative images showing the thoracic cavity upon re-entry, delineating the presence of adhesions between the myocardium or implanted patch and chest wall. Each photograph is annotated to identify the heart, chest wall, and position of the implanted patch, with the specific sites of adhesion indicated by arrows. (**B**) Quantitative analysis of the incidence of surgical adhesion, expressed as a percentage, among the study cohorts at the 4-week endpoint, with sample sizes (n≥5) for each group. (**C**) Representative images of empty patch and TIMED therapeutic patch at 4 weeks post-implantation. H&E staining (left) shows denser cellular infiltrates in empty patches compared with reduced infiltration and more preserved myocardial structure in TIMED patches (scale bar = 50 μm). Immunofluorescence for α-actinin (green) and CD68 (red) (right) demonstrates increased $CD68^+$ macrophage presence in empty patches versus reduced accumulation in TIMED patches (scale bar = 50 μm). (**D**) Quantification of infiltrating cell density and $CD68^+$ cell counts in each group. Statistical analysis was performed using an unpaired two-tailed Student's t-test. n=4.*

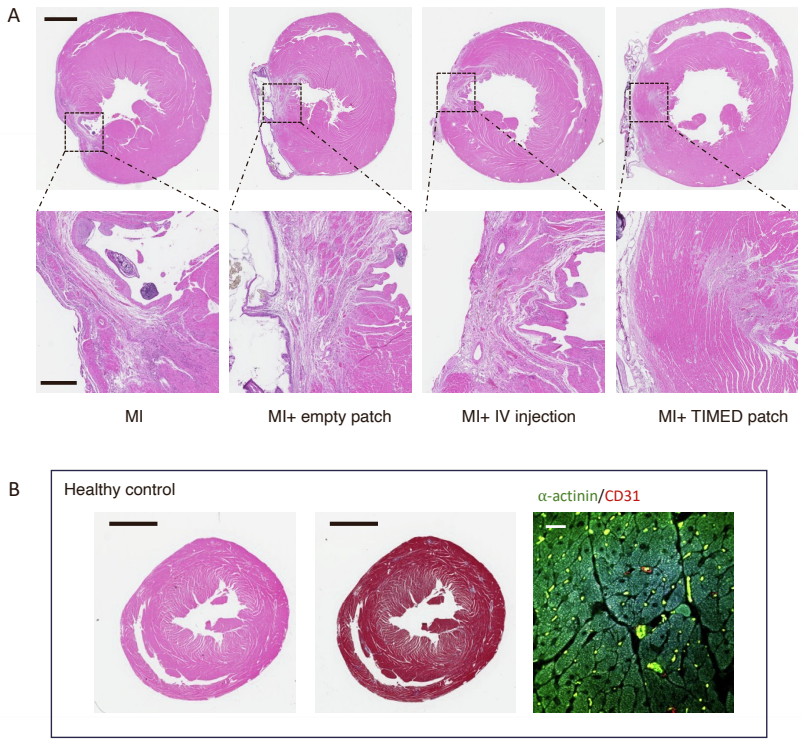

Fig. S18. Histology of cardiac tissues compare to healthy control. *(A) Representative images of H&E staining of the infarct cross-section below the ligation point, showing infarct size in different experimental groups. Scale bar= 5 mm.* ***(B)*** *Representative images of H&E, Masson's trichrome, and immunostaining of the heart sections from a 6-month-old Wistar rat without surgical intervention, serving as a healthy control.*